

Geology, mineralization, and geochronology of the Qianhe gold deposit, Xiong’ershan area, southern North China Craton

Ke-Fei Tang · Jian-Wei Li · David Selby · Mei-Fu Zhou ·
Shi-Jian Bi · Xiao-Dong Deng

Received: 8 January 2012 / Accepted: 17 December 2012 / Published online: 19 January 2013
© Springer-Verlag Berlin Heidelberg 2013

Abstract The Qianhe gold deposit in the Xiong’ershan area is located along the southern margin of the Archean-Paleoproterozoic North China Craton. The deposit consists of six orebodies that are hosted in Paleoproterozoic andesites to basaltic andesites and structurally controlled by roughly EW-trending faults. Individual orebodies comprise auriferous quartz veins and disseminated Au-bearing pyrite within hydrothermally altered rocks on both sides of, or close to, the veins. Ore-related hydrothermal alteration has produced various mixtures of K-feldspar, quartz, sericite, chlorite, epidote, carbonate, and sulfides. Pyrite is the most important ore mineral, associated with minor amounts of galena, sphalerite, and chalcopyrite. Other trace minerals include molybdenite, arsenopyrite, scheelite, rutile, xenotime, and parisite. Gold occurs mostly as native gold and electrum enclosed in pyrite or along microfractures of sulfides and quartz. Microthermometric measurements of

primary inclusions in auriferous quartz suggest that gold and associated minerals were precipitated in the range of 160–305 °C from aqueous or carbonic-aqueous fluids with salinities of 6–22 wt% NaCl equiv. Samples of molybdenite coexisting with Au-bearing pyrite have Re–Os model ages of 134–135 Ma, whereas ore-related hydrothermal sericite separates yield $^{40}\text{Ar}/^{39}\text{Ar}$ plateau ages between 127 and 124 Ma. The Re–Os and $^{40}\text{Ar}/^{39}\text{Ar}$ ages are remarkably consistent with zircon U–Pb ages (134.5 ± 1.5 and 127.2 ± 1.4 Ma; 1σ) of the biotite monzogranite from the Heyu-intrusive complex and granitic dikes in and close to the Qianhe gold mine, indicating a close temporal and thus possibly genetic relationship between gold mineralization and granitic magmatism in the area. Fluid inclusion waters extracted from auriferous quartz have δD values of -80 to -72 ‰, whereas the calculated $\delta^{18}\text{O}_{\text{H}_2\text{O}}$ values range from 3.1 to 3.8 ‰. The hydrogen and oxygen isotopes from this study and previous work indicate that ore fluids were likely derived from degassing of magmas, with addition of minor amounts of meteoric water. Gold mineralization at Qianhe is temporarily coincident with pervasive bimodal magmatism, widespread fault-basin formation, and well development of metamorphic core complexes in the whole eastern North China Craton that have been interpreted as reflecting reactivation of the craton in the late Mesozoic after prolonged stabilization since its formation in the late Paleoproterozoic. It is therefore concluded that the Qianhe gold deposit formed as a result of this craton reactivation event.

Editorial handling: B. Lehmann

Electronic supplementary material The online version of this article (doi:10.1007/s00126-012-0451-2) contains supplementary material, which is available to authorized users.

K.-F. Tang · J.-W. Li
State Key Laboratory of Geological Processes and Mineral
Resource, China University of Geosciences, Wuhan 430074,
China
e-mail: jwli-cug@hotmail.com

K.-F. Tang · J.-W. Li (✉) · S.-J. Bi · X.-D. Deng
Faculty of Earth Resources, China University of Geosciences,
Wuhan 430074, China
e-mail: jwli-cug@hotmail.com

D. Selby
Department of Earth Sciences, University of Durham, Durham
DH1 3LE, UK

M.-F. Zhou
Department of Earth Sciences, The University of Hong Kong,
Hong Kong, SAR, China

Introduction

Numerous gold deposits in the Xiong’ershan area, southern margin of the North China Craton (NCC), are hosted in Neoproterozoic high-grade metamorphic rocks or late Paleoproterozoic volcanic rocks (Mao et al. 2002; Chen et al. 2004). Many deposits have been extensively described in

the last two decades (Fan et al. 1993, 1998; Mao et al. 2002; Lu et al. 2004a; Yang et al. 2003; Han et al. 2007; Chen et al. 2008a, 2009), but their origins remain debated or not well understood. Previous radiometric dating, mostly by K–Ar and Rb–Sr methods, bracketed the gold mineralization at between 595 and 87 Ma (Li and Qu 1993; Qiang et al. 1993; Ren et al. 1996, 2001; Lu et al. 2004b). The large scatter of those “ages” has complicated the understanding of the timing, genesis, and geodynamic setting of gold mineralization in the region. Lu et al. (1999, 2003) and Chen et al. (2008a; 2009) proposed that gold deposits in the Xiong’ershan area formed in the late Triassic to early Jurassic, associated with the evolution of the Triassic Qinling Orogen. In contrast, Mao et al. (2003, 2008a) and Yang et al. (2003) favored that they were results of late Jurassic to early Cretaceous extension or lithospheric thinning of the North China Craton. Precise isotopic dating is crucial to better understand the genesis and tectonic setting of the region-wide gold metallogenesis.

Being one of the largest gold deposits in the Xiong’ershan area, the Qianhe gold deposit (Fig. 1) has been a major focus of previous studies (Li et al. 1999; Pei et al. 2006; Cao 2007; Mao 2008; Wang et al. 2008a), but its formation age, source of ore fluids, and genesis are still poorly understood. Previous Rb–Sr dating of hydrothermal sericite and fluid inclusion waters extracted from Au-bearing quartz veins yielded inconsistent isochron ages of 99.3 ± 6.3 Ma (Qiang et al. 1993) and 155.2 ± 6.6 Ma (Ren et al. 1996), respectively. The large discrepancy in these ages makes it impossible to precisely time gold precipitation and reasonably constrain the ore genesis. In this paper, we present high-precision Re–Os, $^{40}\text{Ar}/^{39}\text{Ar}$, and U–Pb ages in order to place tight constraints on the timing of gold mineralization and to examine the possible relationship between granitoid magmatism and ore formation. We further use fluid inclusion and stable isotope data to characterize and fingerprint the source of the ore fluids. Lastly, the geodynamic setting under which the Qianhe gold deposit was produced is discussed by integrating existing geological and geochronological data from other deposits in the Xiong’ershan area and other parts of the eastern North China craton.

Geological background

The Xiong’ershan area lies in the southern margin of the NCC (insert of Fig. 1). It is bounded by the Machaoying Fault to the south and the Luoning Fault to the northwest (Fig. 1). The area is lithologically dominated by amphibolite-facies metamorphic rocks of the late Archean to early Palaeoproterozoic Taihua Group, which are unconformably overlain by intermediate to silicic volcanic rocks of the Palaeoproterozoic Xiong’er Group (Chen et al. 2009;

Mao et al. 2010; Fig. 1). The Taihua Group consists chiefly of sillimanite–garnet quartz gneiss, graphite gneiss, TTG (tonalite–trondhjemite–granite) gneiss, marble and amphibolite (Xu et al. 2009). The amphibolite and TTG gneiss have whole-rock Sm–Nd and zircon U–Pb age of 2.5–2.3 Ga (Kröner et al. 1988; Xue et al. 1995; Xu et al. 2009). The Xiong’er Group, up to 7,000 m in thickness and covering an area of >6000 km², is widely distributed in the southern NCC (Peng et al. 2008; Zhao et al. 2009). Rocks of the Xiong’er Group consist of basaltic andesite and andesite with minor dacite and rhyolite. These rocks have SHRIMP and LA-ICP-MS zircon U–Pb ages of 1.80–1.75 Ga (Zhao et al. 2004; Peng et al. 2008; He et al. 2009). Mesozoic and Cenozoic redbeds are locally present in the area (Fig. 1).

Several major granitoid intrusions, mainly the Huashan, Wuzhangshan, and Heyu plutons, intrude the Archean and Palaeoproterozoic rocks (Fig. 1). The Huashan pluton consists of monzogranite, granodiorite, and granite, with the monzogranite having a SHRIMP zircon U–Pb age of 132.0 ± 1.6 Ma (Mao et al. 2010). The Wuzhangshan pluton consists of hornblende granite, syenogranite, and granosyenite, and has a SHRIMP zircon U–Pb age of 156.8 ± 1.2 Ma (Mao et al. 2010). The Heyu pluton, with an outcrop of 784 km², intrudes andesite and dacite of the Xiong’er Group immediately to the south of the Qianhe gold deposit and along the Machaoying Fault (Fig. 1). It is composed of four intrusive units that have similar composition. These are fine-, medium- and coarse-grained porphyritic biotite monzonite and fine-grained biotite syenogranite, with zircon U–Pb ages ranging from 148.2 to 127.2 Ma (Guo et al. 2009; Gao et al. 2010; Mao et al. 2010). The age data confirm that the Heyu pluton was produced by multiple episodes of magmatism. A recent geochemical study shows that the Heyu pluton was generated from partial melting of ancient basaltic lower crust in an extensional setting (Guo et al. 2009). Several granite to syenogranite dykes intrude both the Heyu pluton and the adjacent andesite of the Xiong’er Group. Dikes in the Qianhe mine are in general strongly altered forming secondary K-feldspar, pyrite, sericite, and quartz. The Xiong’ershan area also hosts a number of porphyritic granite to granodiorite stocks, many of which are Mo mineralized forming economically important deposits, including the world-class Leimengou (Fig. 1), Shangfanggou and Nannihu Mo deposits (Li 2005). These deposits have molybdenite Re–Os ages of 157–136 Ma (Li et al. 2003a, 2006a).

A number of WNW- and NE-striking faults are developed in the Xiong’ershan area (Mao et al. 2002; Yan et al. 2005). The WNW-trending Machaoying Fault is more than 200 km long and 5 km wide, and dips 50–80° to NNE (Yan et al. 2005; Han et al. 2009). Interpretation of geophysical data suggests that the Machaoying Fault is a transcrustal fracture penetrating into the lithospheric mantle (Yan et al. 2005). To the north of the Machaoying Fault, there are a number of NE-trending secondary or higher-order faults

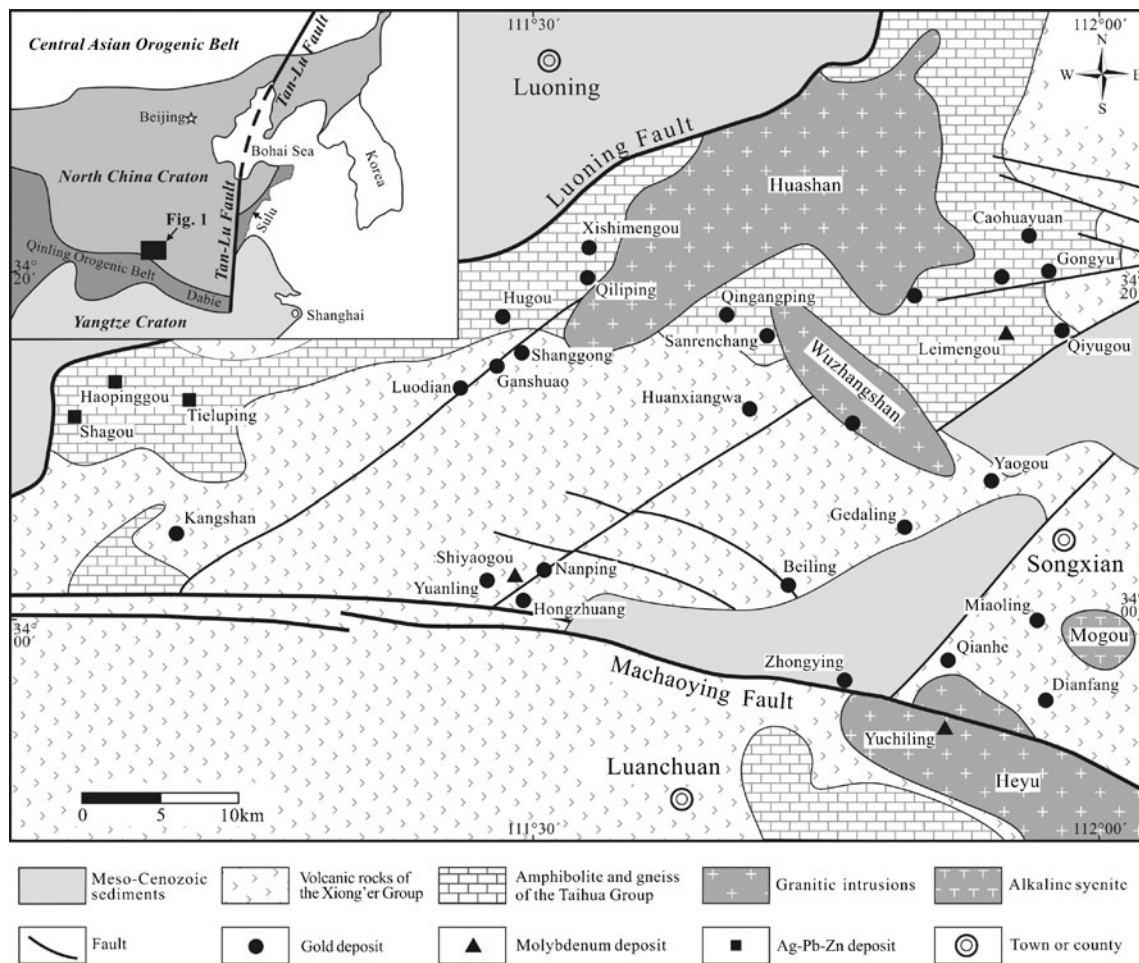


Fig. 1 Geological map of the Xiong'er shan area showing the distribution of major gold deposits (modified from Lu et al. 2004b). Major porphyry Mo and Ag–Pb–Zn vein-type deposits are also shown. Mineralized

porphyry stocks are not shown due to their small exposures (generally <0.5 km²). The *insert* shows tectonic divisions in the eastern China continental margin and the location of the Xiong'er shan

(Fig. 1). To the northwest of the area, the Luoning Fault separates late Mesozoic sedimentary sequences from Archean metamorphic rocks (Qi and Li 2005). The Machaoying and Luoning Faults are considered to have played an important role in the formation and distribution of gold deposits in the area (Fig. 1; Chen and Fu 1992).

Mineralization and alteration

The Qianhe gold deposit (33°59'32" to 33°59'58"N, 111°51'46" to 111°52'36"E), about 45 km southwest of the Songxian County, Henan Province, was discovered in the early 1980s. Mineralization is hosted in andesite and, less significantly, rhyolite and dacite of the Xiong'er Group. Orebodies are largely restricted to alteration zones developed along the WNW-striking F₄ fault and its secondary structures (Figs. 2 and 3). The F₄ fault is approximately 3,800 m long and 5–30 m wide, striking from 275–290° and dipping 55–75° to NNE or NNW. Protomylonite, cataclasite, fault breccias, and

fault gouge are well developed in the fault, indicating multiple deformational events under different structural regimes (Zhang et al. 2006; Han et al. 2009).

The deposit consists of six orebodies, and the mineralization features can be best represented by the largest no. 1 orebody. This orebody strikes 95–110° and dips 58–76° to NE, and is approximately 830 m long, 1.5 to 15 m thick, continuous for more than 320-m-down plunge from the 520- to 200-m elevations (Fig. 3). It exhibits vertical variations in morphology, pattern, and texture, and is locally displaced by post-mineralization faults (Fig. 3a). Gold ores consist of quartz–sulfide veins and stockworks (Fig. 4a) and, less significantly, sulfide disseminations in alteration assemblages (Fig. 4b). Most quartz–sulfide veins occur in the shallow levels, whereas sulfide disseminations tend to be present at lower levels. Individual veins are mostly 30 to 80 cm wide and commonly show laminated textures marked by multiple pyrite veins or stringers in quartz (Fig. 4a). Fracture-veining textures (Fig. 4a, c) indicate syn-mineralization deformation.

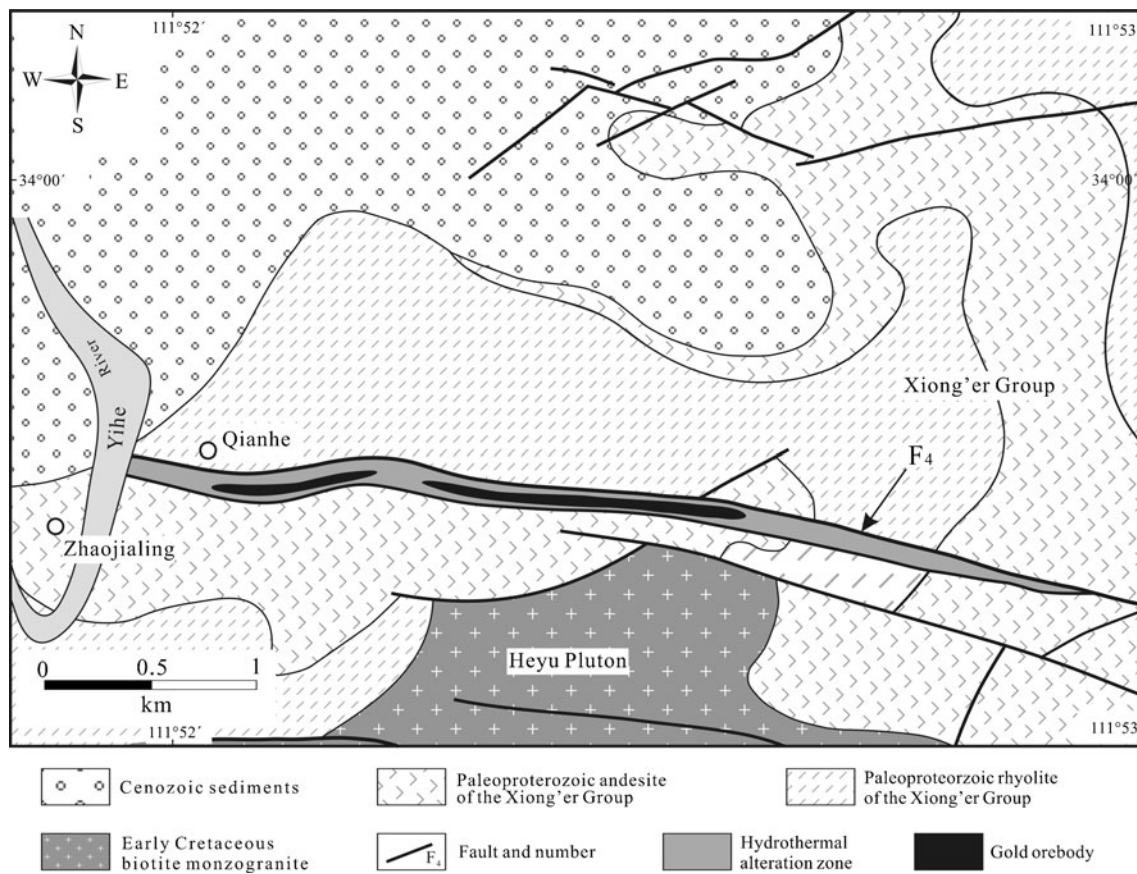
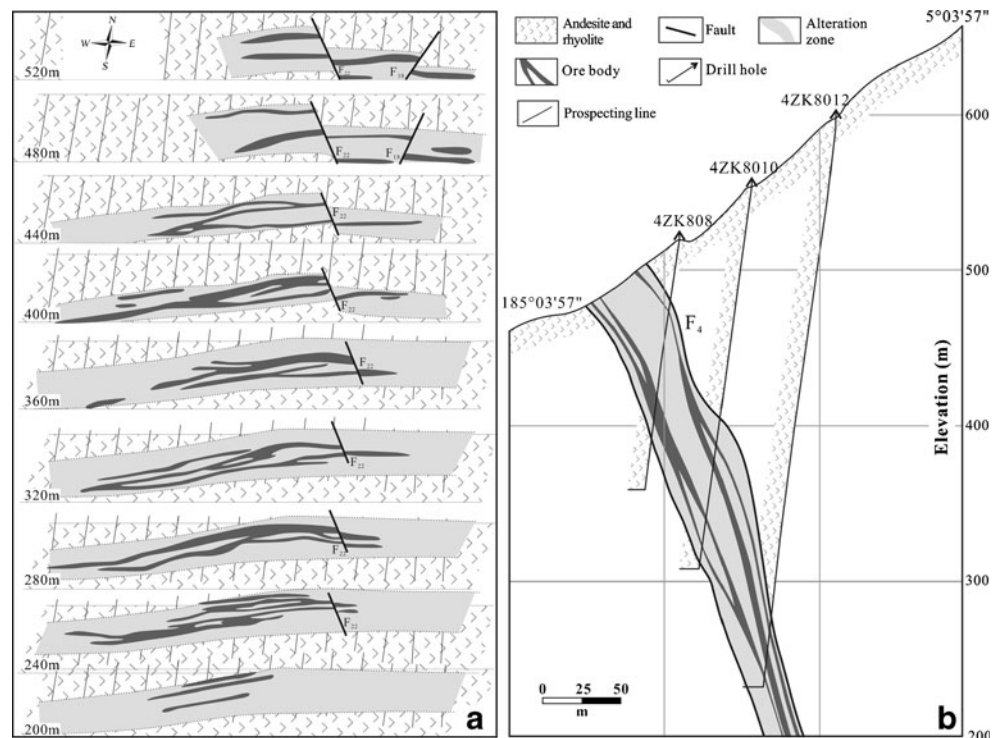


Fig. 2 Simplified geological map of the Qianhe gold deposit (Anonymous 2002, unpublished)

Fig. 3 a Geological plans of various mining levels showing the morphological features of structural controls on gold orebodies. Note that extensive hydrothermal alteration is developed in and along the structural zones. Morphological variations of the orebodies along a vertical axis are also shown (Anonymous 2002, unpublished). **b** A representative cross-section showing the occurrence, morphology and geometry of the largest orebody I from the Qianhe gold deposit (Anonymous 2002, unpublished)



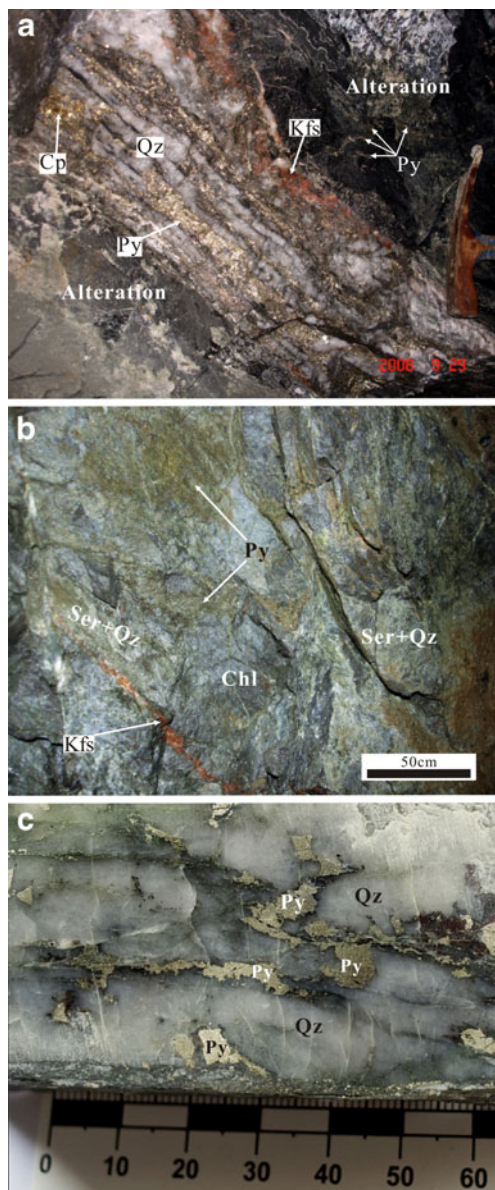


Fig. 4 Photographs showing the occurrences and textures of gold ores. **a** Pyrite in quartz veins as fracture infillings; **b** mineralization in alteration zone consisting of disseminations and patches of pyrite coexisting with sericite, quartz and chlorite; **c** irregular pyrite veins in quartz. Mineral abbreviations: *Py* pyrite, *Qz* quartz, *Kfs* K-feldspar, *Cp* chalcopyrite, *Ser* sericite, *Chl* chlorite, *Ep* epidote

Pyrite is the predominant sulfide mineral, but minor galena and sphalerite and trace amounts of chalcopyrite, molybdenite, argentite, and arsenopyrite are also present (Figs. 5a–d). Barite, scheelite, apatite, rutile and other minor or trace minerals are included in, or coexist with, pyrite (Figs. 5e, f). Gold occurs as native gold and electrum. Native gold commonly forms anhedral grains included in pyrite and quartz, along boundaries between or within microfractures of these two minerals (Figs. 5g, h). Electrum typically occurs as stringers or irregular inclusions within sulfides or quartz (Fig. 5i). Electron microprobe analyses show that native gold consists

of 83–96 wt% Au and 4.4–16.5 wt% Ag, corresponding to a gold fineness of 835–956, whereas the electrum has 54–79 wt% Au and 20–46 wt% Ag, with a gold fineness of 541–796 (Ba et al. 2006).

Hydrothermal alteration is well-developed and largely controlled by the F_4 fault zone (Figs. 2 and 3). The alteration zone ranges in width from 10 to 50 m and contains variable amounts of disseminated pyrite and other metallic minerals. The alteration involved a combination of silicification, sericitization, pyritization, and carbonatization (Fig. 6). Potassic alteration, chloritization, and epidotization are also recognized (Figs. 6a, b, e, f). Potassic alteration is characterized by the presence of disseminated or massive K-feldspar distributed in strongly altered rocks or as irregular K-feldspar veins marginal to quartz veins (Figs. 4a, 6a, b, d, e). K-feldspar grains may be variably replaced by sericite or kaolinite (Figs. 6a, b). Silicification occurs as quartz veins and stockworks, or as quartz aggregates coexisting with sericite and pyrite (Figs. 4b and 6a, c). Sericite is the second most common alteration mineral in mineralized zones and frequently associated with pyrite and quartz (Fig. 6b, c). Chloritization and epidotization are developed in andesites of the Xiong'er Group, generally distal to orebodies (Fig. 6e, f). Carbonization is widespread and represents the late stage of hydrothermal evolution, as indicated by calcite veinlets cross-cutting quartz veins and other alteration phases (Fig. 6d, e). Skarn-like assemblages consisting of garnet, epidote, diopside, actinolite, and magnetite, overprinted by pyrite and calcite, are locally present in the western portion of the alteration zone (Wang et al. 2008a). Gold is closely related to the quartz + sericite + pyrite alteration assemblage.

Three hydrothermal stages can be recognized based on field and petrographic relations (Fig. 7). The first-stage (stage I) formed milky, massive quartz, K-feldspar, and skarn-like minerals. Rare metallic minerals associated with this stage include rutile, scheelite, arsenopyrite, and molybdenite. The second stage (stage II) is best represented by the quartz + sericite + pyrite assemblage and pyrite veins filling fractures in quartz of stage I. Other sulfide minerals and gold also formed predominantly in this stage. Calcite and lesser amounts of fluorite characterize the last stage (stage III).

Samples and analytical methods

Fluid inclusion microthermometry

Fluid inclusion study was conducted for four quartz samples collected from the no. I orebody. Quartz from these samples is intergrown with pyrite and considered as product of mineralizing stage II. Polished thin sections were examined under transmitted light to identify the shape, size, phase, distribution and possible origin of fluid inclusions. Microthermometric measurements were conducted using a British Linkham

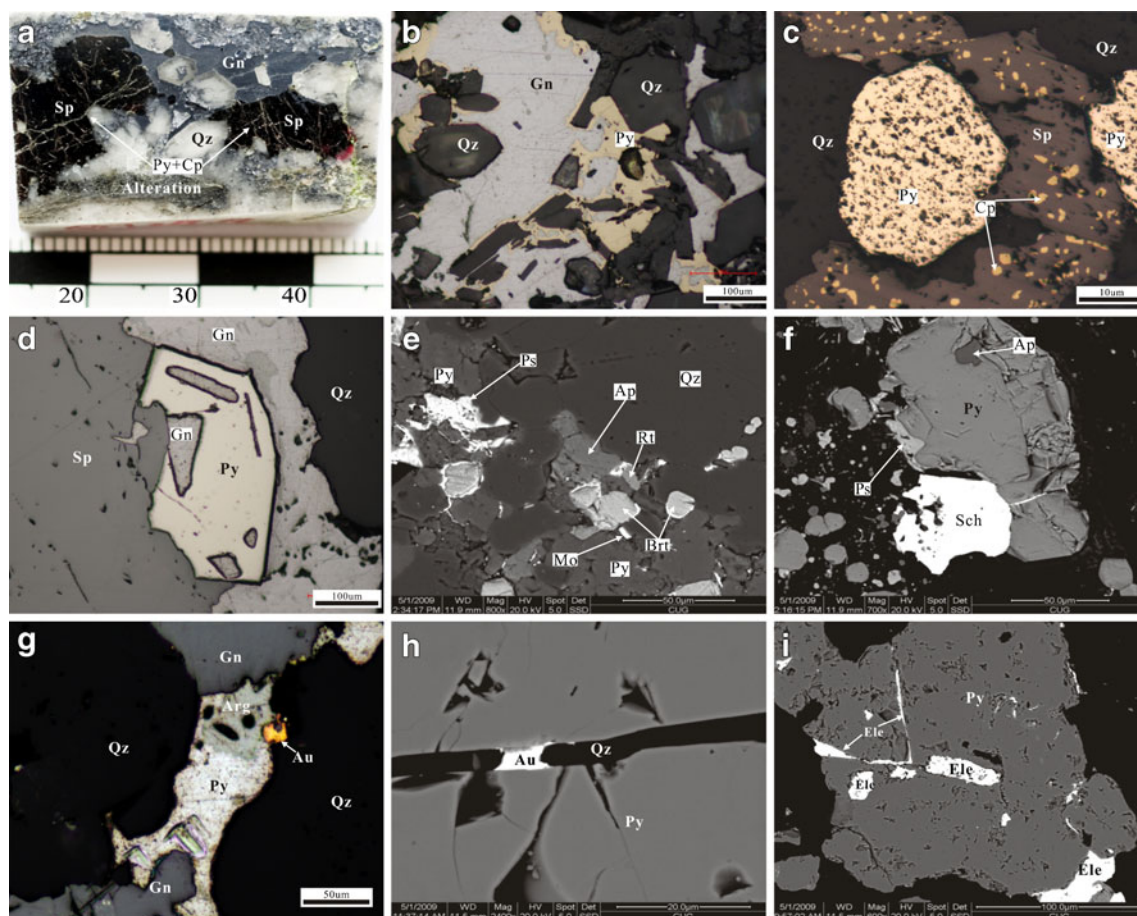


Fig. 5 Photograph (a), reflected-light photomicrographs (b, c, d), and back-scattered electron images (e, f) showing the mineral paragenesis of the Qianhe gold deposit. **a** Sphalerite and galena coexisting with quartz, but crosscut by pyrite and chalcopyrite veinlets. **b** Pyrite replaced by galena. **c** Porous pyrite cut by irregular sphalerite vein containing a solid-solution inclusion of chalcopyrite. **d** Galena is replaced by pyrite and sphalerite. **e** Minor minerals in gold ores including barite, parisiite, apatite, rutile, and molybdenite. **f** Parisiite

and scheelite intergrown with pyrite that contains apatite inclusions. **g** Native gold as interstitial grain between pyrite, argentite and quartz. **h** Gold filling fractures in quartz that cuts pyrite. **c** Electrum inclusions and stringers in porous pyrite. **i** An irregular electrum grain enclosed in quartz. Mineral abbreviations: *Py* pyrite, *Qz* quartz, *Cp* chalcopyrite, *Gn* galenite, *Sp* sphalerite, *Ps* parisiite, *Ap* apatite, *Rt* rutile, *Mo* molybdenite, *Brt* barite, *Sch* scheelite, *Au* native gold, *Arg* argentite, *Ele* electrum

THMS-600 heating–freezing stage on an Olympus BX51 microscope. The uncertainties for the measurements are ± 0.5 , ± 0.2 , and ± 2 °C for runs in the range of -120 to -70 , -70 to 100 , and 100 to 600 °C, respectively. Laser Raman spectroscopic analyses of selected inclusions were carried out with a British Renishaw 1000 Laser Raman spectrometer with a 514-nm Ar-ion laser as the source of excitation.

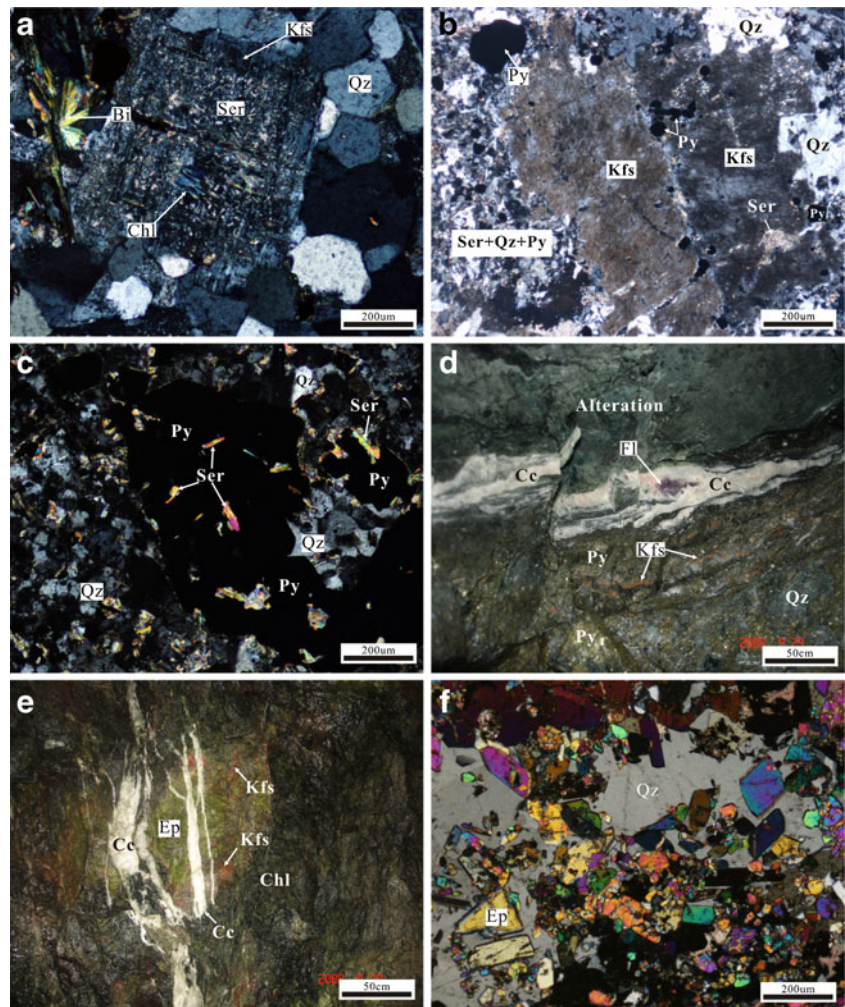
LA-ICP-MS zircon U–Pb dating

Gold orebodies are spatially associated with the Heyu pluton and a number of granitic dikes, dating of the pluton and dikes and ore-related alteration minerals therefore provide age constraints on gold mineralization and examine the possible genetic relationships between ore formation and granitic magmatism. Previous studies have obtained precise zircon U–Pb ages for the Heyu pluton (Gao et al. 2010; Mao

et al. 2010), but the ages of the granitic dikes spatially related to gold orebodies are unknown. Two samples (Q29-1, Q30-19), each from different dikes, were collected for U–Pb dating. Zircons were separated using conventional heavy-liquid and magnetic techniques and then screened under a binocular microscope. Representative grains were mounted in an epoxy resin disk, polished, cleaned, and gold coated. Prior to isotopic analysis, all zircon grains were examined and photographed under transmitted- and reflected-light, and then imaged by cathodoluminescence (CL) to reveal their internal structures.

Zircon U–Pb dating was conducted by LA-ICP-MS at the State Key Laboratory of Geological Processes and Mineral Resources, China University of Geosciences, Wuhan. Detailed operating conditions have been described in Liu et al. (2008a). A GeoLas 2005 laser ablation system was connected to an Agilent 7500a ICP-MS instrument. Off-line

Fig. 6 Photomicrographs (a–c, f) and photographs (d, e) showing common alteration minerals in the Qianhe gold deposit. **a** K-feldspar, coexisting with quartz and biotite, is altered to sericite. The potassic alteration is commonly distal to the gold ores. **b** Sericitic alteration formed through consumption of precursor hydrothermal K-feldspar. Abundant pyrite was precipitated during the alteration. **c** Alteration assemblages consisting of pyrite, quartz and sericite are commonly found in or close to orebodies. Such assemblages are good indicators of mineralization. **d** Late-stage calcite and fluorite veins in close proximity to gold mineralization. **e** Late-stage calcite veins crosscutting chloritization and epidotization generally distal to orebodies. **f** Epidote distal to orebodies replaced by quartz. Mineral abbreviations: *Py* pyrite, *Qz* quartz, *Kfs* K-feldspar, *Ser* sericite, *Chl* chlorite, *Ep* epidote, *Bi* biotite, *Cc* calcite, *Fl* fluorite



selection and integration of background and analytical signals, and time-drift correction and quantitative calibration for trace element analyses and U–Pb dating were performed using ICPMSDataCal (Liu et al. 2008a; Liu et al. 2010). Zircon 91500 was used as an external standard for U–Pb dating, and was analyzed twice every five unknown analyses. Time-dependent drifts of U–Th–Pb isotopic ratios were corrected using a linear interpolation (with time) for every five analyses according to the variations of 91500 (i.e., 2 zircon 91500+5 samples+2 zircon 91500) (Liu et al. 2010). Preferred U–Th–Pb isotopic ratios used for 91500 are from Wiedenbeck et al. (1995). Uncertainty of preferred values for the external standard 91500 was propagated to the ultimate results of the samples. Concordia diagrams and weighted mean calculations were made using Isoplot/Ex_ver 3 (Ludwig 2003).

Re–Os and $^{40}\text{Ar}/^{39}\text{Ar}$ dating

Two samples, QHN02 and QHN04, were taken from underground sites for molybdenite separation. Molybdenite from both samples coexists with quartz, pyrite, and minor amounts of galena, sphalerite, or chalcopyrite. Field relationships

indicate that molybdenite in both samples represents the first stage of mineralization. The Carius tube method was used for dissolution of molybdenite and equilibration of the sample and tracer Re and Os (Selby and Creaser 2001). Approximately 22–23 mg of molybdenite were dissolved and equilibrated with a known amount of ^{185}Re and isotopically normal Os at 240 °C for a 24-h period. Solvent extraction and microdistillation was used to isolate Os, whereas anion exchange chromatography was used to isolate Re (Selby and Creaser 2001). The concentrations of ^{187}Re and ^{187}Os were determined at the Northern Centre for Isotopic and Elemental Tracing Facility, Durham University, using isotope dilution-negative thermal ionization mass spectrometry (ID-NTIMS). Isolated and purified Re and Os solutions were loaded onto Ni and Pt filaments, respectively, for analysis by a Thermo Finnigan TRITON mass-spectrometer using Faraday collectors. Rhenium and Os concentrations and Re–Os ages were calculated using uncertainties in Re and Os mass-spectrometer measurements, spike and standard Re and Os isotopic compositions, calibration uncertainties of ^{185}Re and ^{187}Os and weighing uncertainties. Ages were calculated using the decay constant $^{187}\text{Re}=1.666\times 10^{-11}\text{ year}^{-1}$ of Smoliar et al. (1996).

Mineral	Stage I	Stage II	Stage III
K-feldspar	Abundant		
Garnet	Minor		
Diopside	Minor		
Actinolite	Minor		
Biotite	Abundant		
Chlorite		Minor	
Rutile	Minor		
Scheelite	Minor		
Arsenopyrite	Minor		
Molybdenite	Minor		
Quartz	Abundant		
Sericite		Abundant	
Pyrite		Abundant	
Native gold		Minor	
Electrum		Minor	
Argentite		Minor	
Galena		Abundant	
Sphalerite		Abundant	
Chalcopyrite		Abundant	
Parisite		Minor	
Xenotime		Minor	
Apatite		Minor	
Calcite			Abundant
Fluorite			Abundant

Abundant Common Minor

Fig. 7 Paragenetic sequence of the Qianhe gold deposit. For more details see text

$^{40}\text{Ar}/^{39}\text{Ar}$ dating was conducted on hydrothermal sericite separated from two samples belonging to the pyrite + quartz + sericite assemblage in the no. I orebody at the 240-m elevation that are interpreted as representing mineralization stage II. Based on petrographic examination, suitable parts of the samples were crushed, repeatedly sieved to obtain uniform grains (0.5–1.5 mm), cleaned in distilled water in an ultrasonic bath for 1 h, and dried. Sericite separates were then handpicked under a binocular microscope. The mineral separates were irradiated along with the ZBH-2506 standard (132.7 ± 0.1 Ma; Wang 1983) for 54 h at the 49-2 reactor, Beijing. After a 4-month cooling period, the samples were analyzed by the $^{40}\text{Ar}/^{39}\text{Ar}$ laser heating method using a GV5400 mass spectrometer equipped with a MIR10-50W CO_2 laser. The analytical procedures are described in Qiu and Jiang (2007). Argon gas was extracted at consecutively higher laser powers. The released gases were purified by two Zr–Al getter pumps operated for 5 to 8 min at room temperature and ca. 450 °C, respectively. The background of the sample hold was lower than 2 mV, which is considerably lower than the signals obtained for the gas fractions (40–200 mV), and thus ensuring precise isotope analyses for the unknown. The $^{40}\text{Ar}/^{39}\text{Ar}$ dating results were calculated

and plotted using the ArArCALC software of Koppers (2002). All dates are reported using 5.543×10^{-10} year $^{-1}$ as the total decay constant for ^{40}K (Steiger and Jäger 1977), and the values for the reactor correction factors are 8.984×10^{-4} for ($^{39}\text{Ar}/^{37}\text{Ar}$) Ca, 2.673×10^{-4} for ($^{36}\text{Ar}/^{37}\text{Ar}$) Ca, and 5.97×10^{-3} for ($^{40}\text{Ar}/^{39}\text{Ar}$) K. The J factors used in the age calculations are 0.0091530 ± 0.0000458 and 0.0092230 ± 0.0000461 , respectively.

Stable isotopes

Three samples were collected from the no. I orebody for quartz separation. All samples consist of variable amounts of quartz, pyrite, sericite, galena, and sphalerite that precipitated from the main mineralization stage. The hydrogen and oxygen isotopes of quartz were measured at the Stable Isotope Laboratory of the Institute of Mineral Resources, Chinese Academy of Geological Sciences (CAGS). Hydrogen isotope ratios of bulk fluid inclusions in quartz were measured by mechanically crushing quartz grains of about 5 g, approximately 1 mm in size, according to the method described by Simon (2001). Samples were first degassed of labile volatiles and secondary fluid inclusions by heating under vacuum to 120 °C for 3 h. The subsequently released water was trapped, reduced to H_2 by zinc at 410 °C (Friedman 1953), and then analyzed with MAT-253 mass spectrometer. Analyses of standard water samples suggest a precision for δD of ± 3 ‰ (1σ). Oxygen was liberated from quartz by reaction with BrF_5 (Clayton and Mayeda 1963) and converted to CO_2 on a platinum-coated carbon rod. The $\delta^{18}\text{O}$ determinations were made on a MAT-253 mass spectrometer. The reproducibility for pure, isotopically homogeneous quartz is about ± 0.2 ‰ (2σ) (Li et al. 2010a).

Four pyrite and one galena samples were selected for sulfur isotope analysis. Pyrite and galena grains from the main mineralization stage were handpicked under a binocular microscope. Contamination of mineral separates by other minerals was minimized by selecting coarse-grained grains. The sulfur isotopic analyses were conducted at CAGS, using a conventional off-line method. Approximately 15 mg of pyrite or galena were homogenized with 150 mg of Cu_2O , combusted at 1050 °C for 15 min under vacuum for a quantitative conversion to sulfur dioxide (SO_2) and analyzed for sulfur isotope composition on a MAT 251 mass spectrometer. The sulfur isotope results are generally reproducible within ± 0.2 ‰ (2σ).

Results

Fluid inclusions

The gold-bearing quartz grains contain abundant primary fluid inclusions, which generally have negative crystal, oval or round shapes, with minor strip, triangular and irregular

varieties. Individual inclusions range in size mostly from 2 to 10 μm . Three types of inclusions are recognized on the basis of phases at room and subzero temperatures, textural relationships and laser Raman spectroscopic results (Fig. 8): one-phase aqueous inclusions (type 1), two-phase aqueous inclusions (type 2), and three-phase CO_2 -rich inclusions (type 3). Type 1 inclusions are commonly 2–4 μm in diameter, liquid only, and composed predominantly of H_2O (Fig. 8a). Type 2 inclusions primarily have oval and negative crystal forms, and range from 4 to 7 μm in diameter (Figs. 8b–e). Individual inclusions consist of liquid H_2O and H_2O -dominated vapor, and the vapor accounts for less than 50 % of the total volume. Type 3 inclusions are locally present and contain liquid H_2O , liquid CO_2 , and CO_2 -dominated vapor. They range in size from 10 to 15 μm and have negative crystal forms (Fig. 8f).

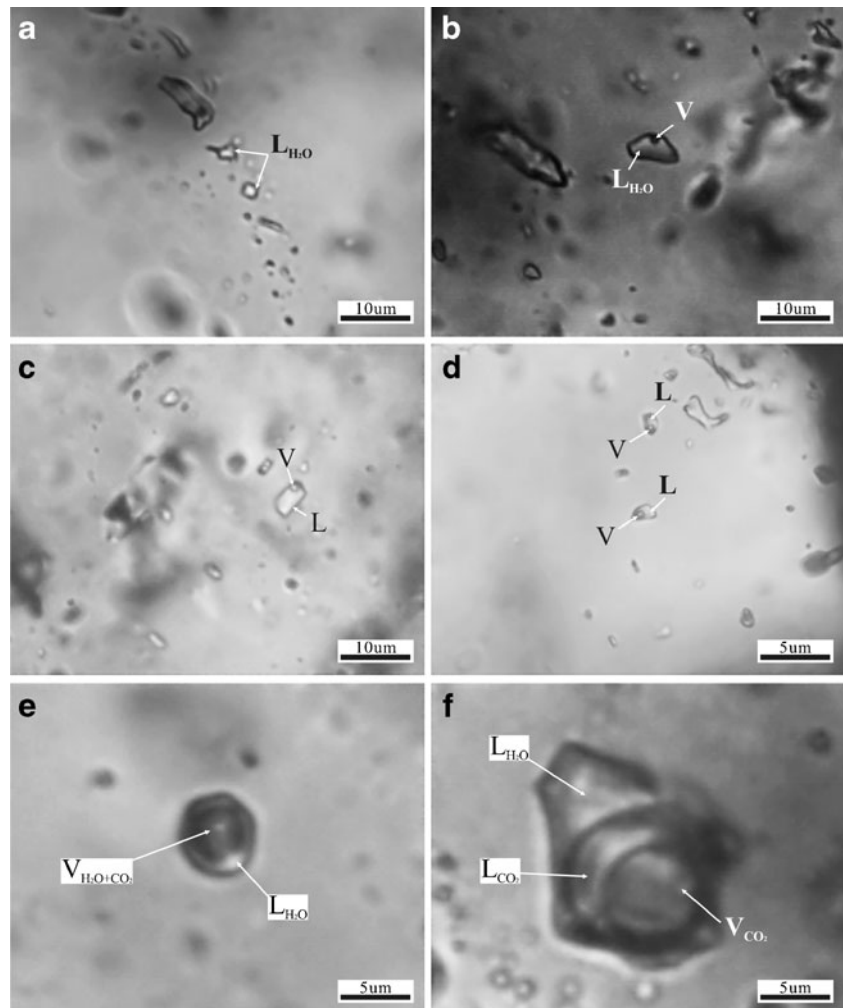
Types 1 and 3 inclusions are too small or rare to be used for microthermometric measurements. The microthermometric data and calculated parameters for type 2 inclusions are summarized in Appendix 1 and depicted in Fig. 9. These inclusions have ice-melting temperatures ($T_{\text{m,ice}}$) between -18.3 and -3.7 $^\circ\text{C}$ and total homogenization temperatures of 160 to

305 $^\circ\text{C}$, with two peaks at 200–240 and 280 $^\circ\text{C}$. All inclusions were finally homogenized into a liquid phase. Their salinities range from 6.1 to 21.8 wt% NaCl equivalent, calculated with $T_{\text{m,ice}}$ values and the equations of Hall et al. (1988). Using the equations of Zhang and Frantz (1987), bulk densities of the ore fluids are estimated to be 0.8–1.0 g/cm^3 . The Raman spectroscopic results show that both the liquid and vapor phases are dominated by H_2O , with minor amounts of CO_2 and traces of CH_4 in the vapor phase (Fig. 10).

Zircon U–Pb ages

Zircon U–Pb isotope data are presented in Appendix 2, and the U–Pb concordia diagrams are shown in Fig. 11. Zircon grains from both samples are euhedral to subhedral, 100–160 μm long, with aspect ratios of 1.5 to 2.5, and commonly characterized by oscillatory zoning. They have high Th and U contents (>500 ppm), with Th/U ratios ranging from 0.49 to 1.32 (Q29-1) and 0.31 to 0.68 (Q30-19) (Appendix 2), typical of magmatic zircons. Fifteen spot analyses on 15 zircon grains from sample Q29-1 yield concordant ages with

Fig. 8 Photomicrographs showing the types, morphologies, and distribution of fluid inclusions. **a** One-phase, liquid-only aqueous inclusions. **b–d** Isolation of liquid-rich, two-phase aqueous inclusions. **e** CO_2 -rich two-phase aqueous-carbonic inclusion. **f** CO_2 -rich, three-phase aqueous-carbonic inclusion with negative crystal form



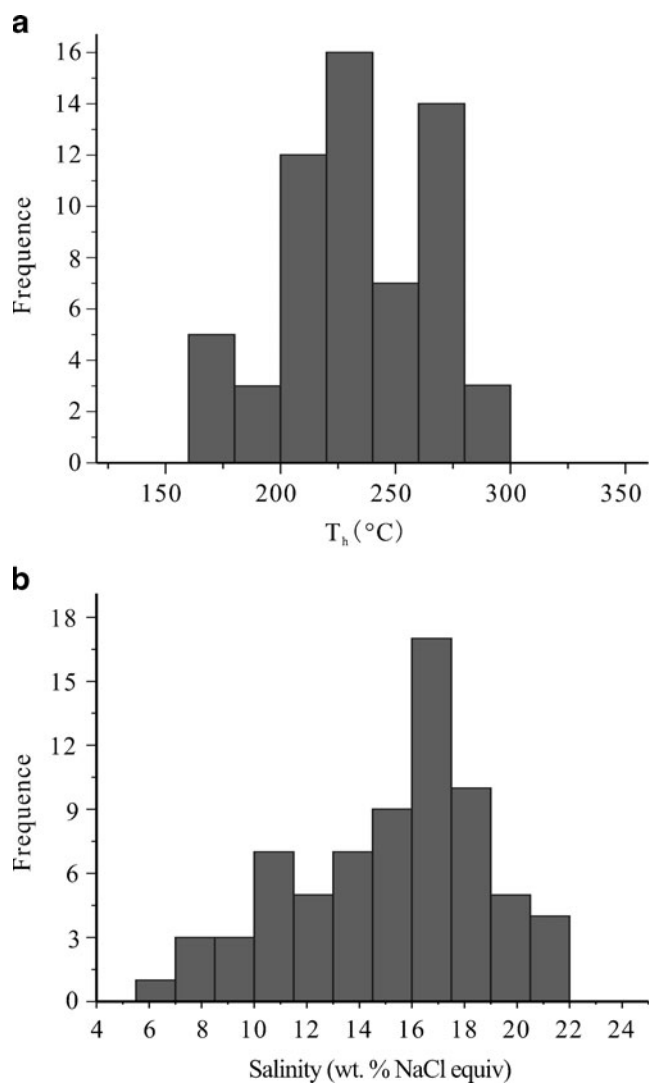


Fig. 9 Histogram of total homogenization temperatures (T_h) (a) and calculated salinities (b) of fluid inclusions from the Qianhe gold deposit

a weighted mean $^{206}\text{Pb}/^{208}\text{U}$ age of 132.6 ± 0.7 Ma (Fig. 11). A total of 15 spot analyses were made on 15 zircon grains for sample Q30-19. Fourteen grains are concordant, with the remaining one being slightly discordant (Fig. 11). However, the discordant analysis has a $^{206}\text{Pb}/^{208}\text{U}$ age indistinguishable from the concordant ones (Appendix 2), indicating that the discordance reflects uncertainties related to ^{207}Pb measurement and common Pb correction, rather than lead loss. All 15 analyses give a weighted mean $^{206}\text{Pb}/^{208}\text{U}$ age of 132.8 ± 0.6 Ma (1σ). The U–Pb ages of both samples are interpreted as the time of crystallization of the granitic dikes in the mine.

Re–Os and $^{40}\text{Ar}/^{39}\text{Ar}$ ages

Two molybdenite separates contain 30.2–33.9 ppm Re and 42.6–47.9 ppb ^{187}Os , and have similar Re–Os model ages of

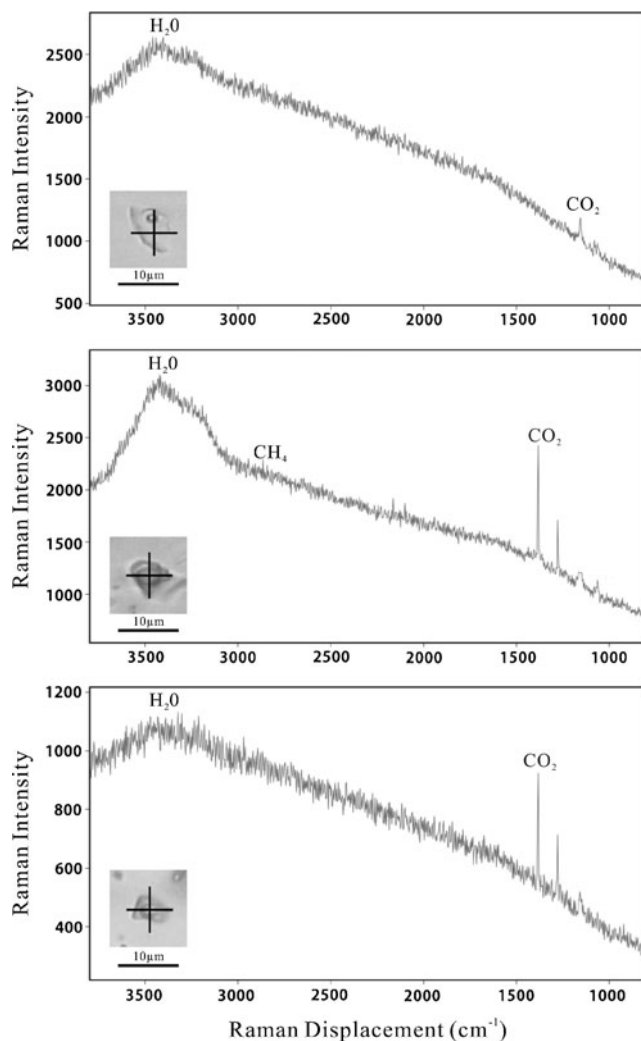


Fig. 10 Raman spectra of fluid inclusions indicating presence of variable amounts of CO_2 , both in the vapor and liquid phases

134.5 ± 0.6 and 134.7 ± 0.6 Ma (2σ ; Table 1). The ages are interpreted as the crystallization age of the molybdenite.

$^{40}\text{Ar}/^{39}\text{Ar}$ data of sericite separates are summarized in Appendix 3, and the apparent age spectra are illustrated in Fig. 12. Sample QH29 has a well-defined plateau age of 127.0 ± 1.6 Ma, comprising 12 continuous steps that account for 90 % of the total ^{39}Ar released. The initial two heating steps have younger apparent ages with larger errors corresponding to smaller percentages of radiogenic ^{40}Ar , indicating very minor argon loss in the outermost part of the mineral after its crystallization. The plateau age is within errors of the integrated age (equivalent to a K–Ar age; 125.2 ± 1.2 Ma), confirming that the sample contained no excess argon. Sample Q240 is characterized by an ascending spectrum with younger apparent ages at the low to medium temperature steps, indicating minor argon loss. The spectrum reaches a plateau consisting of eight high temperature steps, with a plateau age of 123.8 ± 1.3 Ma. The integrated

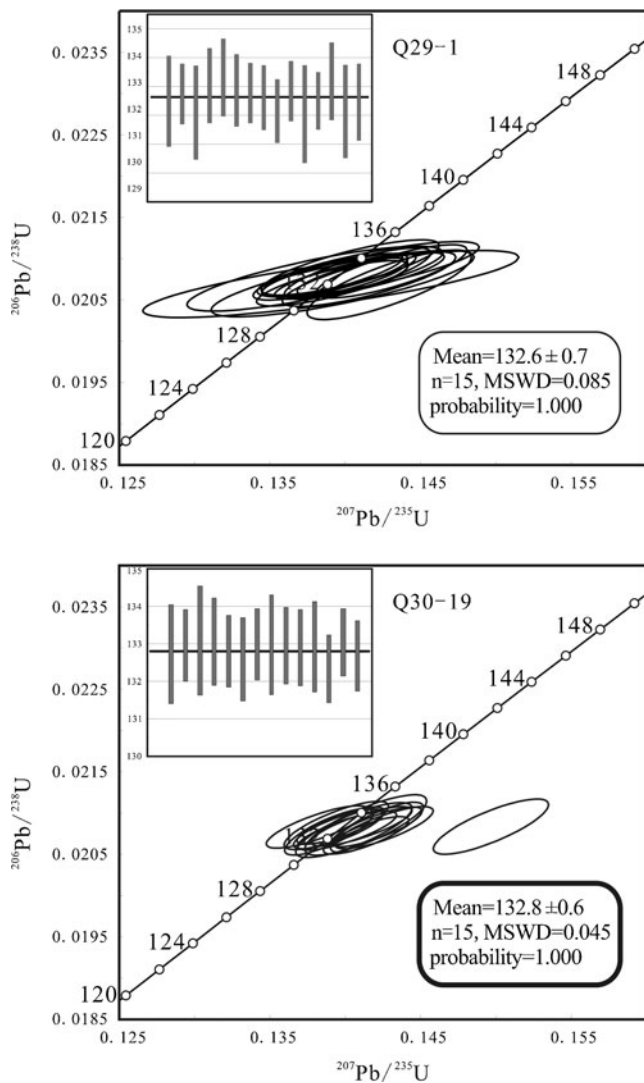


Fig. 11 U–Pb concordia diagrams of zircons from two granitic dikes in the mining area

age (119.0 ± 1.2 Ma) is slightly younger than the plateau age, consistent with minor argon loss as indicated by the shape of the apparent age spectrum.

Stable isotopes

Hydrogen and oxygen isotopes

Hydrogen and oxygen isotope data of gold-bearing quartz samples are listed in Appendix 4 and plotted in

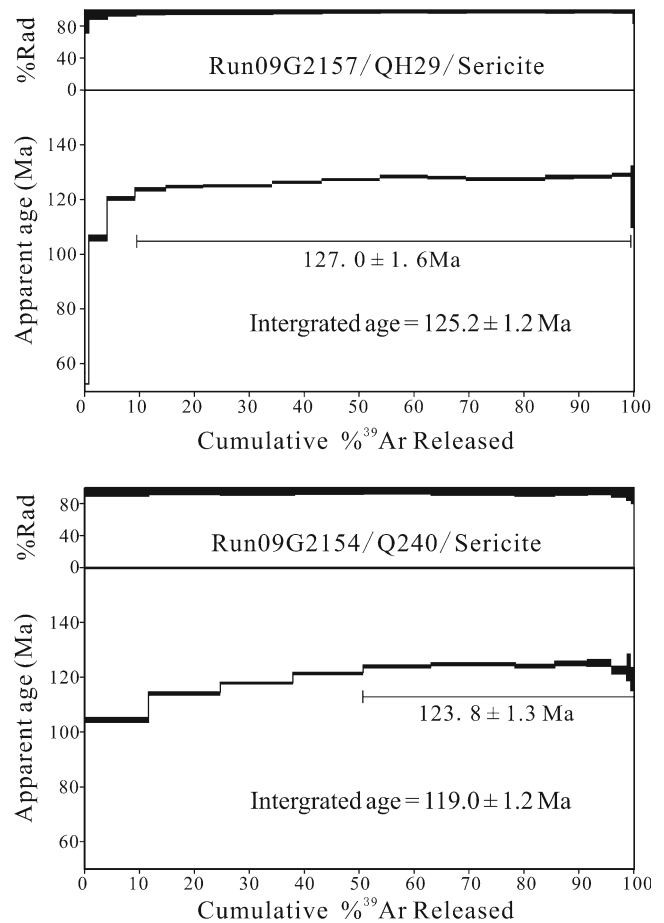


Fig. 12 $^{40}\text{Ar}/^{39}\text{Ar}$ age spectra of ore-related sericite from the Qianhe gold deposit

Fig. 13. Hydrogen and oxygen isotope data of the Qiyugou breccia pipe gold deposit from the western Xiong’ershan Area (Fig. 1), which is contemporaneous with the Qianhe gold deposit, are also included in Fig. 13. Quartz separates have $\delta^{18}\text{O}_{\text{V-SMOW}}$ values of 10.8 to 11.5 ‰, whereas fluid inclusion waters extracted from quartz have $\delta\text{D}_{\text{H}_2\text{O}}$ values ranging from -80 to -72 ‰. The $\delta^{18}\text{O}_{\text{V-SMOW}}$ values of ore fluids were calculated using the quartz–water equilibrium function of Clayton et al. (1972), assuming a mineralizing temperature of 280 °C based on the final homogenization temperatures of primary fluid inclusions (Fig. 9). The calculations yield $\delta^{18}\text{O}_{\text{V-SMOW}}$ of 3.1 to 3.8 ‰ for the mineralizing fluids (Appendix 4), which is consistent with results of previous studies (4.4 to 5.0 ‰; Li et al.

Table 1 Re–Os isotope data of molybdenite from the Qianhe gold deposit

Sample no.	Weight (g)	Re (ppm)	$\pm 2\sigma$	^{187}Re (ppm)	$\pm 2\sigma$	^{187}Os (ppb)	$\pm 2\sigma$	Age (Ma)	$\pm 2\sigma$
QHN02	0.022	30.2	0.1	19.0	0.1	42.6	0.1	134.5	0.6
QHN04	0.023	33.9	0.1	21.3	0.1	47.9	0.1	134.7	0.6

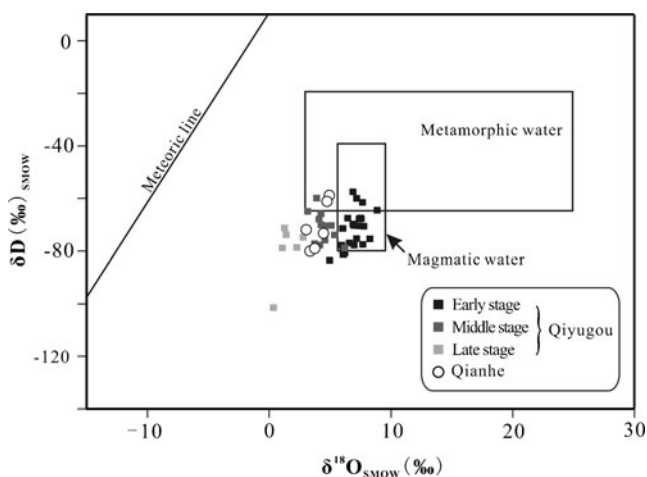


Fig. 13 δD versus $\delta^{18}O$ diagram for ore fluids of the Qianhe and Qiyugou gold deposits in the Xiong'ershan area. For location of the Qiyugou deposit, see Fig. 1. Isotope data of the Qiyugou deposit are from Chen et al. (2009) and Fan et al. (2011), whereas the reference fields for the magmatic and metamorphic waters and the meteoric line are from Taylor (1974)

1999; Yan et al. 2005). In the $\delta^{18}O$ vs. δD diagram (Fig. 13), the samples plot in an area transitional from the magmatic field to the meteoric line, but in closer proximity to the magmatic component.

Sulfur isotopes

Two pyrite separates have $\delta^{34}S$ values of 0.26 and -0.08 ‰, whereas the other two have negative values of -6.7 and -10.6 ‰, respectively (Appendix 4). One galena sample has a more negative $\delta^{34}S$ value of -16.3 ‰. Several previous studies reported similar sulfur isotope compositions for pyrite, with $\delta^{34}S$ values ranging from -14.8 to 2.8 ‰ (Appendix 4; Fig. 14; Anonymous (2002) The exploration report of Qianhe gold deposit, Henan Province, in China, unpublished; Lu et al. 2003; Yan et al. 2005).

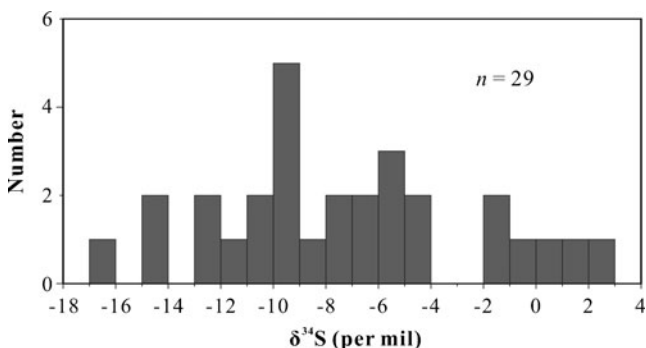


Fig. 14 Histogram of $\delta^{34}S$ values of gold-related sulfide minerals from the Qianhe gold deposit. Data are from Lu et al. (2003), Yan et al. (2005), Anonymous (2002, unpublished), and this study

Discussion

Timing of mineralization

Molybdenite Re–Os chronometer is remarkably robust due to the high closure temperature of Re–Os isotopes in molybdenite (Suzuki et al. 1996; Stein et al. 2001). Thus, Re–Os dating of this mineral commonly provides reliable constraints on the timing of ore formation (Selby et al. 2002). Two molybdenite separates from the Qianhe gold deposit, which are closely associated with gold-bearing pyrite, have reproducible Re–Os model ages of 134.7 ± 0.6 and 134.5 ± 0.6 Ma (Table 1), providing the first reliable constraints on the age of the Qianhe gold deposit.

Field and petrographic relations (Fig. 6c) indicate that sericite is closely related to gold mineralization, and thus $^{40}Ar/^{39}Ar$ dating of sericite provides additional constraints on the timing of hydrothermal alteration and gold deposition. Two sericite samples have broadly consistent plateau ages (Fig. 12), which are interpreted as the cooling age of the samples below the closure temperature of argon diffusion in white mica (300 – 350 °C; McDougall and Harrison 1999). Microthermometric measurements of primary fluid inclusions from auriferous quartz samples yielded final homogenization temperatures mostly between 300 and 200 °C (Fig. 9), lower than the argon closure temperature for white mica at moderate cooling rates (McDougall and Harrison 1999). Consequently, the sericite $^{40}Ar/^{39}Ar$ ages can also be considered as the mineralization age for the Qianhe gold deposit. Thus, the present Re–Os and $^{40}Ar/^{39}Ar$ ages may indicate two discrete mineralizing events in the early Cretaceous. Two separate mineralizing events are consistent with the multiple episodes of intrusive magmatism recorded by the Heyu pluton (see below).

The difference between the Re–Os and $^{40}Ar/^{39}Ar$ ages can also be explained to reflect a slow cooling history of the mineralizing system from ca. 135 – 134 Ma (molybdenite Re–Os ages) to 127 – 124 Ma (sericite $^{40}Ar/^{39}Ar$ ages). Alternatively, the $^{40}Ar/^{39}Ar$ ages may simply represent resetting of the K–Ar system in sericite that was crystallized at 135 – 134 Ma. Samples from the northern and central parts of the Heyu Pluton (Fig. 1) have concordant U–Pb ages of 134.5 ± 1.5 Ma (Guo et al. 2009) and 127.2 ± 1.1 Ma (Mao et al. 2010), which are equivalent to the present Re–Os and $^{40}Ar/^{39}Ar$ ages, respectively. It is inferred that either gold mineralization was related to the early magmatism and then disturbed by the late-stage intrusion, or that the gold deposits were generated by two separate hydrothermal events related to the repeated magmatic pulses. Two granitic dikes emplaced at ca. 132 – 133 Ma in the mining area are broadly contemporaneous with the early intrusion of the Heyu Pluton, and are considered to be genetically related to gold mineralization (see below).

A possible magmatic affinity

The fluid inclusions in quartz samples from the main mineralization stage have salinities ranging from 22 to 6 wt% NaCl equivalent with an average of 15.3 wt% NaCl equivalent (Fig. 9). The values are much higher than salinities of metamorphic fluids responsible for lode gold deposits in many Precambrian cratons worldwide (Groves et al. 1998; Goldfarb et al. 2005; Klein et al. 2008), but are consistent with a magmatic component (Lang and Baker 2001; Baker et al. 2006). The hydrogen and oxygen isotopes of auriferous quartz samples from the Qianhe deposit plot close to the magmatic field in the δD versus $\delta^{18}O_{SMOW}$ diagram, and are comparable with ore samples of the Qiyugou breccia pipe gold deposit (Fig. 13). The Qiyugou deposit (Fig. 1) has a molybdenite Re–Os isochron age (135.6 ± 5.6 Ma; Yao et al. 2009) identical to the Re–Os ages of the Qianhe gold deposit, indicating that they formed in the same metallogenic event. Field and petrographic relations indicate an early, middle, and late stages for the Qiyugou deposit, with gold being precipitated in the first two stages (Chen et al. 2009). Fluid inclusion and stable isotope data confirm that ore fluids of the early stage were dominated by a magmatic component, with addition of meteoric water in the middle and late stages (Chen et al. 2009; Fan et al. 2011). The similar δD and $\delta^{18}O_{SMOW}$ values between the Qianhe gold deposit and the middle-stage samples of the Qiyugou deposit (Fig. 13) provide additional argument for a magmatic source of the ore fluids generating the Qianhe gold deposit.

Six pyrite separates have $\delta^{34}S$ values close to zero (Appendix 4; Fig. 14), indicating a deep-seated, most likely magmatic source for the sulfur (Ohmoto 1972). On the other hand, other pyrite and galena samples have negative $\delta^{34}S$ values ranging from -16.3 to -6.7 ‰ (Fig. 14). The negative isotopic values either reflect a sulfur source from an anoxic environment or isotopic fractionation in the evolution of the mineralizing fluids. Because no organic sulfur has been found from any lithological unit in the Xiong’ershan area, we suggest that the negative $\delta^{34}S$ compositions are unlikely a source characteristic, rather they are most probably related to oxidation of the ore fluid system. The presence of barite, scheelite, pargasite, and apatite (Fig. 5e, f) confirm oxidizing conditions in the ore fluids in the early stage of mineralization. The proposed fluid oxidation can be explained by extensive interaction of hydrothermal fluids with the Fe^{2+} -rich andesite in the Xiong’er Group, as indicated by pervasive alteration in and around the orebodies (Figs. 2–4). Such interactions are linked to the consumption of reduced aqueous S in the formation of pyrite and oxidation of the mineralizing fluids (Lambert et al. 1984). As a consequence of fluid oxidation, the residual fluids, and thus the sulfide minerals precipitated from the fluids, would be ^{32}S -enriched, accounting for the negative

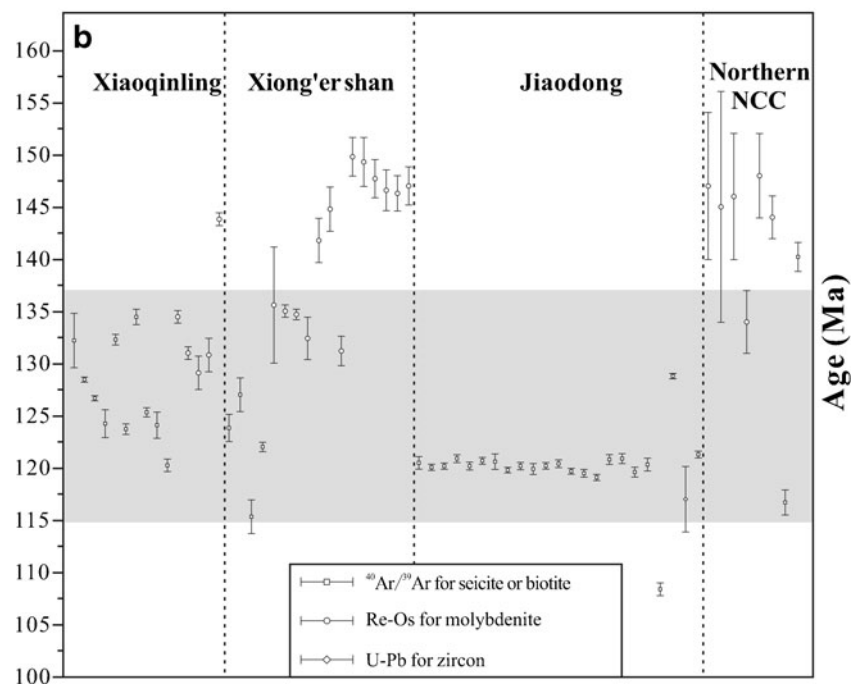
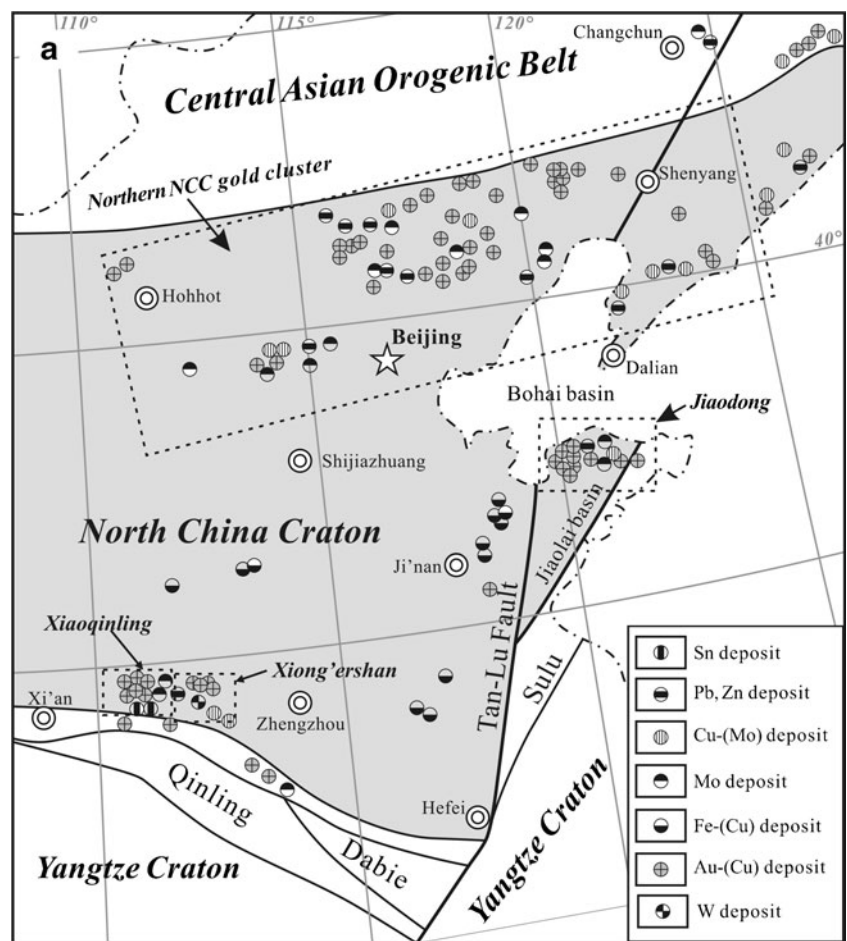
$\delta^{34}S$ values. Collectively, the $\delta^{34}S$ data close to zero is consistent with a magmatic source, whereas the negative $\delta^{34}S$ values are the result of fluid oxidation. The compatible molybdenite Re–Os ages for gold ores (134.5–134.7 Ma; Table 1) and zircon U–Pb age for granitic dikes (132.6–132.8 Ma; Fig. 11) in the mining area and one biotite monzogranite sample from the Heyu pluton (134.5 Ma; Guo et al. 2009) are also consistent with a magmatic origin of the Qianhe gold deposit. Both the granitic dikes and andesites of the Xiong’er Group close to the dikes were intensively altered forming sericite + quartz + sulfide assemblages, indicating magmatic devolatilization associated with the emplacement of the dikes and, by inference, the Heyu pluton. Widespread skarn-like assemblages in the western segment of the Qianhe deposit, consisting of garnet, epidote, diopside, actinolite, magnetite, pyrite and calcite, may have also resulted from metasomatism of the Paleoproterozoic andesites by a magmatic fluid (Wang et al. 2008a).

The synchronicity of the regional magmatism and mineralization provide an additional argument for a magmatic derivation of the ore fluids and other components. Geochronological data have revealed that pervasive Au, Mo, and Ag–Pb–Zn mineralization throughout the Xiong’ershan area (Fig. 1) occurred predominantly in the 145 to 115 Ma interval (Wang et al. 2001; Li et al. 2003a; 2005; Qi and Li 2005; Han et al. 2007; Mao et al. 2008a; Yao et al. 2009; Zhou et al. 2009), coincident with the emplacement of granitic intrusions and numerous mineralized porphyry stocks in the area (158–110 Ma; Li 2005; Wang et al. 2005; Han et al. 2007; Mao et al. 2008a; Ye et al. 2008; Guo et al. 2009; Gao et al. 2010). Extensive magmatism could have provided sufficient heat energy, fluids and other components contributing to the formation of gold and other types of deposits throughout the area.

Regional synthesis and geodynamic setting

Immediately to the west of the Xiong’ershan area, the Xiaoqinling area (Fig. 15a) contains more than 40 gold deposits with proven gold reserves of approximately 800 t (Yang et al. 2003). Previous Re–Os and $^{40}Ar/^{39}Ar$ dating indicates that the Dongchuang, Hongtuling, and Qianjiayu gold deposits formed between 132 and 127 Ma (Xu et al. 1998; Wang et al. 2002; Li et al. 2007). More recently, Li et al. (2012a, b) provided a comprehensive geochronological study on major gold deposits in Xiaoqinling, bracketing their formation in the range of 154–119 Ma. These data thus indicate synchronous gold deposition in the Xiong’ershan and Xiaoqinling areas. Gold mineralization in both areas is coeval with the emplacement of the Xiaoqinling metamorphic core complex (135–123 Ma; Zhang and Zheng 1999) and intrusion of many mafic dikes and A-type granites

Fig. 15 **a** Sketch diagram showing distribution of major gold deposits and contemporaneous polymetallic deposits in the eastern North China Craton, modified from Wu et al. (2005) and Mao et al. (2003). **b** Summary of radiometric ages for gold and polymetallic deposits in the eastern North China Craton. Data from Huang et al. (1996, 2009), Xu et al. (1998), Wang et al. (2001, 2002, 2010), Wei et al. (2001), Li et al. (2003b, 2006b), Li et al. (2003a, 2005), Zhang et al. (2003), Hu et al. (2004, 2006), Guo et al. (2006), Li et al. (2007), Wang et al. (2008b), Yao et al. (2009), Zhou et al. (2009), Li et al. (2010b), Li et al. (2012a, 2012b), and this study



(141–117 Ma; Ye et al. 2008; Zhou et al. 2008; Mao et al. 2010; Wang et al. 2011; Li et al. 2012b), indicating that gold

deposits both in the Xiong'er shan and Xiaoqinling areas formed in an extensional setting.

Early Cretaceous lode gold deposits are also widespread in the Jiaodong gold province and other parts of the eastern NCC (Fig. 15a) (Pei 1998; 2003; Mao et al. 2008b). The Jiaodong district (Fig. 15a) is the largest gold repository in China, containing proven reserves of >1,000 t Au (Qiu et al. 2002). Recent detailed geochronological studies have demonstrated that a majority of the gold deposits were emplaced at approximately 120 Ma (Yang et al. 2000; Li et al. 2003b, 2006b), with a few deposits having ages of 108–107 Ma (Li et al. 2006b). Gold veining in Jiaodong was accompanied with the emplacement of numerous mafic dikes and fault-basin formation, indicating an extensional setting for gold mineralization (Davis et al. 2002; Ren et al. 2002; Liu et al. 2006a, 2008b; Mao et al. 2008b; Tan et al. 2008; Li et al. 2011; Zhang et al. 2011). A large number of Au, Mo (Cu), and skarn Fe (Cu) deposits in the northern margin of the NCC (Fig. 15a) have ages of 148–112 Ma (Huang et al. 1996; Wei et al. 2001; Yu and Mao 2004; Mao et al. 2005; Zheng et al. 2007; Wang et al. 2008b). The broadly contemporaneous mineralization in the southern, eastern and northern parts of the NCC strongly suggests a craton-wide gold metallogenic event under consistent geodynamic setting (Fig. 15b).

After prolonged stabilization since its formation in the late Paleoproterozoic (Zhao et al. 2009), the NCC was significantly reactivated in the Mesozoic as indicated by extensive magmatism (Guo et al. 2001; Wu et al. 2005; Zhang et al. 2005; Gao et al. 2008). Many zircon U–Pb geochronological studies have shown that the magmatism took place mostly in the late Jurassic to early Cretaceous (158–120 Ma), an event interpreted in terms of extension or thinning of the subcontinental mantle lithosphere beneath the NCC (Xu et al. 2004; Wu et al. 2005; Mao et al. 2010; Yan et al. 2010). Lithospheric extension of the NCC is further illustrated by the development of numerous metamorphic core complexes (Davis et al. 2002; Liu et al. 2006b, 2008c; Zhu et al. 2007, 2010) and intra-continental rift basins (Tian et al. 1992; Ren et al. 2002), with the former being precisely dated at 130–110 Ma (Zhang and Zheng 1999; Davis et al. 2002; Liu et al. 2005; Yang et al. 2007). Recent geophysical data provide more compelling evidence for a loss of at least 80–120 km of the lithosphere beneath the eastern NCC (Chen et al. 2008b). We therefore conclude that pervasive gold mineralization throughout the eastern NCC was ultimately controlled by the removal and thinning of mantle lithosphere beneath the craton. The mechanism of this lithospheric thinning event is debatable, but may have involved delamination of the lithosphere associated with upwelling of asthenosphere during the late Mesozoic when the paleo-Pacific plate was westerly subducted underneath the eastern Eurasian continent (e.g., Wu et al. 2005; Mao et al. 2011, 2012).

Conclusions

The Qianhe gold deposit formed at intermediate temperature (160–305 °C) from moderately saline fluids with salinities of 22–6 wt% NaCl equivalent. Molybdenite Re–Os and sericite $^{40}\text{Ar}/^{39}\text{Ar}$ dating revealed that the Qianhe gold deposit either formed by two separate mineralizing events at 135–134 and ca. 127 Ma, or was thermally disturbed by post-mineralization processes after its formation at 135–134 Ma. Hydrogen and oxygen isotopes of auriferous quartz and sulfur isotopes of sulfide minerals, together with the U–Pb ages of granitic intrusions spatially associated with gold orebodies, favor a possible magmatic derivation for the ore fluids and sulfur.

Gold and polymetallic deposits of similar ages are widespread in several other major orefields along the southern, eastern, and northern edges of the NCC, revealing a craton-wide, relatively short-lived, metallogenic event. This event is temporarily coincident with extensive magmatism, formation of rifted-basins, and development of metamorphic core complex over the NCC, all pointing to extension and reactivation of the NCC. Thus, it is concluded that large-scaled mineralization in the Xiong’ershan area and throughout the eastern NCC was controlled by cratonic reactivation.

Acknowledgments Financial support for this research was provided by the Natural Science Foundation of China (grants 90814004 and 40821061), the Fundamental Research Funds for the Central Universities (CUG120102), and the MOST special fund from the State Key Laboratory of Geological Processes and Mineral Resources (MSFGPMR201205). Prof. Huaning Qiu is thanked for his expert suggestions in the course of $^{40}\text{Ar}/^{39}\text{Ar}$ dating. Zhanke Li and Zhiyuan Ren are thanked for their assistance in the field and during lab work. We are indebted to Mr. Kuang Gongming from the Jinniu Gold Company for his logistic support during our stay at the mine. We thank Prof. Jinwen Mao and an anonymous reviewer for their thorough review and comments that have been very helpful in our revision. Our special thanks go to Prof. Bernd Lehmann for his constructive suggestions in improving the presentation of the paper.

References

- Ba AM, Ma HY, Zhang SS, Tian XQ (2006) Ore characteristics and ore-searching direction of Qianhe gold mine in Songxian County. Henan Province Contributions to Geology and Mineral Resources Research 21:100–114 (in Chinese with English abstract)
- Baker T, Ebert S, Rombach C, Ryan CG (2006) Chemical compositions of fluid inclusions in intrusion-related gold systems, Alaska and Yukon, using PIXE microanalysis. Econ Geol 101:311–327
- Cao Y (2007) Mineral geochemistry and deep prediction of the Qianhe gold mine in Henan. PhD dissertation, China University of Geology Science, Beijing (in Chinese with English abstract)
- Chen YJ, Fu SG (1992) Gold mineralization in West Hennan. Seismological Press, Beijing (in Chinese)
- Chen YJ, Pirajno F, Sui Y (2004) Isotope geochemistry of the Tieluping silver-lead deposit, Henan, China: a case study of orogenic silver-dominated deposits and related tectonic setting. Miner Deposita 39:560–575

- Chen L, Tao W, Zhao L, Zheng TY (2008a) Distinct lateral variation of lithospheric thickness in the Northeastern North China Craton. *Earth Planet Sci Lett* 267:56–68
- Chen YJ, Pirajno F, Qi JP (2008b) The Shanggong gold deposit, Eastern Qinling Orogen, China: isotope geochemistry and implications for ore genesis. *J Asian Earth Sci* 33:252–266
- Chen YJ, Pirajno F, Li N, Guo D, Lai Y (2009) Isotope systematics and fluid inclusion studies of the Qiyugou breccia pipe-hosted gold deposit, Qinling Orogen, Henan province, China: implications for ore genesis. *Ore Geol Rev* 35:245–261
- Clayton RN, Mayeda TK (1963) The use of bromine pentafluoride in the extraction of oxygen from oxides and silicates for isotopic analysis. *Geochim Cosmochim Acta* 27:43–52
- Clayton RN, O'Neil JR, Mayeda TK (1972) Oxygen isotope exchange between quartz and water. *J Geophys Res* 77:3057–3067
- Davis GA, Darby BJ, Yadong Z, Spell TL (2002) Geometric and temporal evolution of an extensional detachment fault, Hohhot metamorphic core complex, Inner Mongolia, China. *Geology* 30:1003–1006
- Fan HR, Xie YH, Wang YL (1993) The properties of magmatic hydrothermal fluid of Huashan granitic batholith in Western Henan Province and their relationship to gold mineralization. *Acta Petrol Sin* 9:136–145 (in Chinese with English abstract)
- Fan HR, Xie YH, Wang YL (1998) Fluid-rock interaction during mineralization of the Shanggong structure-controlled alteration-type gold deposit in Western Henan Province, central China. *Acta Petrol Sin* 14:530–541 (in Chinese with English abstract)
- Fan HR, Hu FF, Wilde SA, Yang KF, Jin CW (2011) The Qiyugou gold-bearing breccia pipes, Xiong'er-shan region, central China: fluid-inclusion and stable-isotope evidence for an origin from magmatic fluids. *Int Geol Rev* 53:25–45
- Friedman I (1953) Deuterium content of natural waters and other substances. *Geochim Cosmochim Acta* 4:89–103
- Gao S, Rudnick RL, Xu WL, Yuan HL, Liu YS, Walker RJ, Puchtel IS, Liu X, Huang H, Wang XR (2008) Recycling deep cratonic lithosphere and generation of intraplate magmatism in the North China Craton. *Earth Planet Sci Lett* 270:41–53
- Gao XY, Zhao TP, Yuan ZL, Zhou YY, Gao JF (2010) Geochemistry and petrogenesis of the Heyu batholith in the southern margin of the North China block. *Acta Petrol Sin* 26:3485–3506
- Goldfarb R, Baker T, Dube B, Groves DI, Hart CJR, Gosselin P (2005) Distribution, character and genesis of gold deposits in metamorphic terranes. In: *Economic Geology One Hundredth Anniversary volume*. Society of Economic Geologists, Littleton, pp. 407–450
- Groves DI, Goldfarb RJ, Gebre-Mariam M, Hagemann SG, Robert F (1998) Orogenic gold deposits: a proposed classification in the context of their crustal distribution and relationship to other gold deposit types. *Ore Geol Rev* 13:7–27
- Guo F, Fan WM, Wang YJ, Lin G (2001) Late Mesozoic mafic intrusive complexes in North China Block: constraints on the nature of subcontinental lithospheric mantle. *Phys Chem Earth Solid Earth Geod* 26:759–771
- Guo BJ, Mao JW, Li HM, Qu WJ, Chou JJ, Ye HS, Li MW, Zhu XL (2006) Re-Os dating of the molybdenite from the Qiushuwan Cu-Mo deposit in the east Qinling and its geological significance. *Acta Petrol Sin* 22:2341–2348 (in Chinese with English abstract)
- Guo B, Zhu LM, Li B, Gong HJ, Wang JQ (2009) Zircon U-Pb age and Hf isotope composition of the Huashan and Heyu granite plutons at the southern margin of North China Craton: implications for geodynamic setting. *Acta Petrol Sin* 25:265–281 (in Chinese with English abstract)
- Hall DL, Sterner SM, Bodnar RJ (1988) Freezing point depression of NaCl-KCl-H₂O solutions. *Econ Geol* 83:197
- Han YG, Li XH, Zhang SH, Zhang YH, Chen FK (2007) Single grain Rb-Sr dating of euhedral and cataclastic pyrite from the Qiyugou gold deposit in western Henan, central China. *Chin Sci Bull* 52:1820–1826
- Han YG, Zhang SH, Pirajno F, Wang Y, Zhang YH (2009) New ⁴⁰Ar/³⁹Ar age constraints on the deformation along the Machaoying fault zone: Implications for Early Cambrian tectonism in the North China Craton. *Gondwana Res* 16:255–263
- He YH, Zhao GC, Sun M, Xia XP (2009) SHRIMP and LA-ICP-MS zircon geochronology of the Xiong'er volcanic rocks: Implications for the Paleo-Mesoproterozoic evolution of the southern margin of the North China Craton. *Precambrian Res* 168:213–222
- Hu FF, Fan HR, Yang JH, Wan YS, Liu DY, Zhai MG, Jin CW (2004) Mineralizing age of the Rushan lode gold deposit in the Jiaodong Peninsula: SHRIMP U-Pb dating on hydrothermal zircon. *Chin Sci Bull* 49:1629–1636 (in Chinese)
- Hu FF, Fan HR, Yang JH, Wang F, Zhai MG (2006) The ⁴⁰Ar/³⁹Ar dating age of sericite from altered rocks in the Rushan lode gold deposit, Jiaodong Peninsula and its constraints on the gold mineralization. *Bull Mineral Petrol Geochem* 25:109–114 (in Chinese with English abstract)
- Huang DH, Du AD, Wu CY, Liu LS, Sun YL, Zou XQ (1996) Metallogeny of molybdenum (-copper) deposits in the North China Platform: Re-Os age of molybdenite and its geological significance. *Miner Depos* 15:365–373 (in Chinese with English abstract)
- Huang DH, Hou ZQ, Yang ZM, Li ZQ, Xu DX (2009) Geological and geochemical characteristics, metallogenetic mechanism and tectonic setting of carbonatite vein-type Mo (Pb) deposits in the East Qinling molybdenum ore belt. *Acta Geol Sin* 83:1968–1984 (in Chinese with English abstract)
- Klein EL, Ribeiro J, Harris C, Moura C, Giret A (2008) Geology and Fluid Characteristics of the Mina Velha and Mandiocall Orebodies and Implications for the Genesis of the Orogenic Chega Tudo Gold Deposit, Gurupi Belt, Brazil. *Econ Geol* 103:957–980
- Koppers AAP (2002) ArArCALC: software for ⁴⁰Ar/³⁹Ar age calculations. *Comput Geosci* 28:605–619
- Kröner A, Compston W, Zhang GW, Guo AL, Todt W (1988) Age and tectonic setting of Late Archean greenstone-gneiss terrain in Henan Province, China, as revealed by single-grain zircon dating. *Geology* 16:211–215
- Lambert LB, Phillips GN, Groves DL (1984) Sulfur isotope compositions and genesis of Archean gold mineralization, Australia and Zimbabwe. In: Foster RP (ed.) *Gold 82: The Geology, Geochemistry and Genesis of Gold Deposits*. Taylor and Francis, Rotterdam, pp. 373–387
- Lang JR, Baker T (2001) Intrusion-related gold systems: the present level of understanding. *Miner Deposita* 36:477–489
- Li YF (2005) The temporal-spital evolution of Mesozoic granitoids in the Xiong'er-shan area and their relationships to molybdenum-gold mineralization. PhD dissertation, China University of Geosciences, Beijing (in Chinese with English abstract)
- Li SM, Qu LQ (1993) The enrichment rule of metallogenetic condition of structure-alternating type of gold deposits and their metallogenetic mode and forecast. *Collection of papers on gold deposits in Qinling and Dabieshan*. Geological Publishing House, Beijing, pp 96–132 (in Chinese)
- Li L, Qing M, Chen X (1999) Geochemical features of Qianhe gold deposit Henan. *Gold Geol* 5:75–80 (in Chinese with English abstract)
- Li JW, Vasconcelos PM, Zhang J, Zhou MF, Zhang XJ, Yang FH (2003a) ⁴⁰Ar/³⁹Ar constraints on a temporal link between gold mineralization, magmatism, and continental margin transtension in the Jiaodong gold province, Eastern China. *J Geol* 111:741–751
- Li YF, Mao JW, Bai FJ, Li JP, He ZJ (2003b) Re-Os isotopic dating of molybdenites in the Nannihu molybdenum (tungsten) orefield in the Eastern Qinling and its geological significance. *Geol Rev* 49:652–659 (in Chinese with English abstract)

- Li JW, Vasconcelos PM, Zhou MF, Zhao XF, Ma CQ (2006a) Geochronology of the Pengjiakuang and Rushan gold deposits, eastern Jiaodong gold province, northeastern China: implications for regional mineralization and geodynamic setting. *Econ Geol* 101:1023–1038
- Li YF, Mao JW, Liu DY, Wang YB, Wang ZL, Wang YT, Li XF, Zhang ZH, Guo BJ (2006b) SHRIMP zircon U-Pb and molybdenite Re-Os datings for the Leimengou porphyry molybdenum deposit, Western Henan and its geological implication. *Geol Rev* 52:122–131 (in Chinese with English abstract)
- Li HM, Ye HS, Mao JW, Wang DH, Chen YC, Qu WJ, Du AD (2007) Re-Os dating of molybdenites from Au(Mo) deposits in Xiaoqinling gold ore district and its geological significance. *Mineral Deposits* 26:417–424 (in Chinese with English abstract)
- Li CM, Deng JF, Chen LH, Su SG, Li HM, Hu SL, Liu XM (2010a) Two periods of zircon from Dongping gold deposit in Zhangjiakou-Xuanhua area, northern margin of North China: Constraints on metallogenic chronology. *Mineral Deposits* 29:265–275 (in Chinese with English abstract)
- Li YH, Hou KJ, Wan DF, Zhang ZJ, Yue GL (2010b) Formation mechanism of precambrian banded iron formation and atmosphere and ocean during early stage of the Earth. *Acta Geol Sin* 84:1359–1373
- Li SG, Zhao GC, Dai LM, Liu X, Zhou LH, Santosh M, Suo YH (2011) Mesozoic basins in eastern China and their bearing on the deconstruction of the North China Craton. *Journal of Asian Earth Sciences* 47:64–79
- Li JW, Bi SJ, Selby D, Chen L, Vasconcelos P, Thiede D, Zhou MF, Zhao XF, Li ZK, Qiu HN (2012a) Giant Mesozoic gold provinces related to the destruction of the North China craton. *Earth Planet Sci Lett* 349–350:26–37
- Li JW, Li ZK, Zhou MF, Chen L, Bi SJ, Deng XD, Qiu HN, Cohen B, Selby D, Zhao XF (2012b) The Early Cretaceous Yangzhaiyu Lode Gold Deposit, North China Craton: a Link between craton reactivation and gold veining. *Econ Geol* 107:43–79
- Liu JL, Davis GA, Lin ZY, Wu FY (2005) The Liaonan metamorphic core complex, Southeastern Liaoning Province, North China: a likely contributor to Cretaceous rotation of Eastern Liaoning, Korea and contiguous areas. *Tectonophysics* 407:65–80
- Liu JL, Guan HM, Ji M, Hu L (2006a) Late Mesozoic metamorphic core complexes: new constraints on lithosphere thinning in North China. *Prog Nat Sci* 16:633–638 (in Chinese)
- Liu S, Zou HB, Hu RZ, Zhao JH, Feng CX (2006b) Mesozoic mafic dikes from the Shandong Peninsula, North China Craton: petrogenesis and tectonic implications. *Geochem J* 40:181–195
- Liu JL, Davis GA, Ji M, Guan HM, Bai XD (2008a) Crustal detachment and destruction of the North China Craton: constraints from Late Mesozoic extensional structures. *Earth Sci Front* 15:072–081 (in Chinese with English abstract)
- Liu S, Hu RZ, Gao S, Feng CX, Qi L, Zhong H, Xiao TF, Qi YQ, Wang T, Coulson IM (2008b) Zircon U-Pb geochronology and major, trace elemental and Sr-Nd-Pb isotopic geochemistry of mafic dykes in western Shandong Province, east China: Constrains on their petrogenesis and geodynamic significance. *Chem Geol* 255:329–345
- Liu YS, Hu ZC, Gao S, Günther D, Xu J, Gao CG, Chen HH (2008c) In situ analysis of major and trace elements of anhydrous minerals by LA-ICP-MS without applying an internal standard. *Chem Geol* 257:34–43
- Liu YS, Gao S, Hu ZC, Gao CG, Zong KQ, Wang DB (2010) Continental and oceanic crust recycling-induced melt–peridotite interactions in the trans-north China Orogen: U–Pb dating, Hf isotopes and trace elements in Zircons from Mantle Xenoliths. *J Petrol* 51:537–571
- Lu XX, Wei XD, Dong Y, Xuan SM (1999) The metallogenic epoch of gold deposits in Xiaoqinling-Xiong’ershan region. *Gold Geol* 5:11–16 (in Chinese with English abstract)
- Lu XX, Wei XD, Yu ZP, Ye AW (2003) Characteristics of ore-forming fluids in gold deposits of Xiaoqinling-Xiong’ershan area. *Miner Depos* 22:377–385 (in Chinese with English abstract)
- Lu XX, Wei XD, Yu ZP, Wang YT, Xue LW, Ye AW, Suo TY, Jin JP (2004a) Minerogenesis of gold and its coupling with tectonics in Xiaoqinling-Xiong’ershan region. *Gold Geol* 10:1–5 (in Chinese with English abstract)
- Lu XX, Wei XD, Dong Y, Yu ZP, Chang QL, Zhang GS, Liu SL, Ye AW, Suo TY, Jin JP (2004b) Characteristics of gold deposits in Xiaoqinling-Xiong’ershan area and its fluids from mantle, central China. Geological Publishing House, Beijing (in Chinese)
- Ludwig KR (2003) ISOPLOT 3.00: a geochronological toolkit for Microsoft Excel. Berkeley Geochronology Center, Berkeley
- Mao FL (2008) Analysis on regularity of ore-controlling structure and metallogenic prognosis of the Qianhe gold deposit in Henan. Master dissertation, China University of Geosciences, Beijing (in Chinese with English abstract)
- Mao JW, Goldfarb RJ, Zhang ZW, Xu WY, Qiu YM, Deng J (2002) Gold deposits in the Xiaoqinling-Xiong’ershan region, Qinling Mountains, central China. *Miner Deposita* 37:306–325
- Mao JW, Zhang ZH, Yu JJ, Wang YT, Niu BG (2003) The geodynamics setting of Mesozoic large-scale mineralization in North China: the revelation from accurate timing of metal deposits. *Sci China Ser D* 33:289–299 (in Chinese)
- Mao JW, Xie GQ, Zhang ZH, Li XF, Wang YT, Zhang CQ, Li YF (2005) Mesozoic large-scale metallogenic pulses in North China and corresponding geodynamic settings. *Acta Petrol Sin* 21:16–188 (in Chinese with English abstract)
- Mao JW, Xie GQ, Bierlein F, Qü WJ, Du AD, Ye HS, Pirajno F, Li HM, Guo BJ, Li YF (2008a) Tectonic implications from Re-Os dating of Mesozoic molybdenum deposits in the East Qinling-Dabie orogenic belt. *Geochim Cosmochim Acta* 72:4607–4626
- Mao JW, Wang YT, Li HM, Pirajno F, Zhang CQ, Wang RT (2008b) The relationship of mantle-derived fluids to gold metallogenesis in the Jiaodong Peninsula: Evidence from D-O-C-S isotope systematics. *Ore Geol Rev* 33:361–381
- Mao JW, Xie GQ, Pirajno F, Ye HS, Wang YB, Li YF, Xiang JF, Zhao HJ (2010) Late Jurassic-Early Cretaceous granitoid magmatism in Eastern Qinling, central-eastern China: SHRIMP zircon U-Pb ages and tectonic implications. *Aust J Earth Sci* 57:51–78
- Mao JW, Pirajno F, Cook N (2011) Mesozoic metallogeny in East China and corresponding geodynamic settings—an introduction to the special issue. *Ore Geol Rev* 43:1–7
- Mao JW, Cheng YB, Chen MH, Pirajno F (2012) Major types and time-space distribution of Mesozoic ore deposits in South China and their geodynamic settings. *Mineralium Deposita*. Doi: 10.1007/s00126-012-0446-z
- McDougall I, Harrison TM (1999) Geochronology and thermochronology by the $^{40}\text{Ar}/^{39}\text{Ar}$ method. Oxford University Press, New York
- Ohmoto H (1972) Systematics of sulfur and carbon isotopes in hydrothermal ore deposits. *Econ Geol* 67:551–578
- Pei RF (1998) Metallogenic series and prospecting of the metal deposits in north margin of the North China Craton. Geological Publishing House, Beijing (in Chinese)
- Pei RF, Mei YX (2003) The evolution of the metallogenic provinces and ore-forming chronology: a case study of the metallogenic province in the northern margin of the north platform and its north side. Geological Publishing House, Beijing, in Chinese with English abstract
- Pei YH, Yan HQ, Zhang MY (2006) Rock and mineral characteristics of Qianhe gold deposit in Henan. *Mineral Resour Geol* 20:513–518 (in Chinese with English abstract)
- Peng P, Zhai MG, Ernst RE, Guo JH, Liu F, Hu B (2008) A 1.78 Ga large igneous province in the North China craton: the Xiong’er volcanic province and the North China dyke swarm. *Lithos* 101:260–280

- Qiu JZ, Li HG (2005) The structure, ore fluid and element geochemistry of the Qiyugou breccia pipe-type gold deposit. Geological Publishing House, Beijing (in Chinese)
- Qiang LZ, Zhao TP, Yuan ZL (1993) New understanding of the ages of Au-Pb-Zn deposits within Xiong'er Group. *Henan Geol* 11:1–1 (in Chinese)
- Qiu HN, Jiang YD (2007) Sphalerite $^{40}\text{Ar}/^{39}\text{Ar}$ progressive crushing and stepwise heating techniques. *Earth Planet Sci Lett* 256:224–232
- Qiu YM, Groves DI, McNaughton NJ, Wang LG, Zhou TH (2002) Nature, age, and tectonic setting of granitoid-hosted, orogenic gold deposits of the Jiaodong Peninsula, eastern North China craton, China. *Miner Deposita* 37:283–305
- Ren FG, Li WM, Li ZH, Zhao JN, Ding SY, Gao YD, Wang GF, Wang ZY, Bai WC, Lei SB (1996) Ore-forming geological conditions and models for ore searching and ore evaluation of gold deposit in Xiongershan-Xiaoshan area. Geological Publishing House, Beijing (in Chinese with English abstract)
- Ren FG, Yin YJ, Li SB, Zhao JN (2001) The coupling character between isotopic geochronology of Indosinian epoch in Xiong'er fault basin. *Bull Mineral Petrol Geochem* 20:286–288 (in Chinese with English abstract)
- Ren JY, Tamaki K, Li ST, Zhang JX (2002) Late Mesozoic and Cenozoic rifting and its dynamic setting in Eastern China and adjacent areas. *Tectonophysics* 344:175–205
- Selby D, Creaser RA (2001) Re-Os geochronology and systematics in molybdenite from the Endako porphyry molybdenum deposit, British Columbia, Canada. *Econ Geol* 96:197–204
- Selby D, Creaser RA, Hart CJR, Rombach CS, Thompson JFH, Smith MT, Bakke AA, Goldfarb RJ (2002) Absolute timing of sulfide and gold mineralization: a comparison of Re-Os molybdenite and Ar-Ar mica methods from the Tintina Gold Belt, Alaska. *Geology* 30:791–794
- Simon K (2001) Does δD from fluid inclusion in quartz reflect the original hydrothermal fluid? *Chem Geol* 177:483–495
- Smoliar MI, Walker RJ, Morgan JW (1996) Re-Os ages of group IIA, IIIA, IVA, and IVB iron meteorites. *Science* 271:1099–1102
- Steiger RH, Jäger E (1977) Subcommittee on geochronology: convention on the use of decay constants in geo- and cosmochronology. *Earth Planet Sci Lett* 36:359–362
- Stein HJ, Markey RJ, Morgan JW, Hannah JL, Scherstén A (2001) The remarkable Re-Os chronometer in molybdenite: how and why it works. *Terra Nova* 13:479–486
- Suzuki K, Shimizu H, Masuda A (1996) Re-Os dating of molybdenites from ore deposits in Japan: implication for the closure temperature of the Re-Os system for molybdenite and the cooling history of molybdenum ore deposits. *Geochim Cosmochim Acta* 60:3151–3159
- Tan J, Wei JH, Guo LL, Zhang KQ, Yao CL, Lu JP, Li HM (2008) LA-ICP-MS zircon U-Pb dating and phenocryst EPMA of dikes, Guocheng, Jiaodong Peninsula: implications for North China Craton lithosphere evolution. *Sci China Ser D Earth Sci* 51:1483–1500
- Taylor HP (1974) The application of oxygen and hydrogen isotope studies to problems of hydrothermal alteration and ore deposition. *Econ Geol* 69:843–883
- Tian ZY, Han P, Xu KD (1992) The Mesozoic-Cenozoic east China rift system. *Tectonophysics* 208:341–363
- Wang SS (1983) Age determinations of ^{40}Ar - ^{40}K , ^{40}Ar - ^{39}Ar and radiogenic ^{40}Ar released characteristics on K-Ar geostandards of China. *Scientia Geologica Sinica*, pp. 315–323
- Wang YT, Mao JW, Lu XX (2001) $^{40}\text{Ar}/^{39}\text{Ar}$ dating and geochronological constraints on the ore-forming epoch of the Qiyugou gold deposit in Songxian County, Henan Province. *Geol Rev* 47:551–555 (in Chinese with English abstract)
- Wang YT, Mao JW, Lu XX, Ye AW (2002) $^{40}\text{Ar}/^{39}\text{Ar}$ dating and geological implication of the auriferous altered rocks from the middle-deep section of the Q875 gold-quartz vein in the Xiaqingling area, Henan, China. *Chin Sci Bull* 47:1750–1755 (in Chinese)
- Wang DY, Pei FP, Xu WL, Wang QH, Yang DB (2005) Chronology of Mesozoic granitoids in the southern margin of the North China Block: evidence from $^{40}\text{Ar}/^{39}\text{Ar}$ dating of hornblende and biotite. *Geotecton Metallog* 29:262–268 (in Chinese with English abstract)
- Wang RH, Jin CZ, Li JC (2008a) $^{40}\text{Ar}/^{39}\text{Ar}$ isotopic dating for Paishanlou gold deposit and its geological implication. *J Northeastern University (Nat Sci)* 29:1482–1485 (in Chinese with English abstract)
- Wang ZC, Li SR, Shen JF (2008b) Skarnization of Qianhe structural alteration type gold deposit in Henan Province and its ore-prospecting significance. *Mineral Deposits* 27:751–761 (in Chinese with English abstract)
- Wang YT, Ye HS, Ye AW, Li YG, Shuai Y, Zhang CQ, Dai JZ (2010) Re-Os age of molybdenite from the Majiawa Au-Mo deposit of quartz vein type in the north of the Xiaqingling gold area and its implication for metallogeny. *Earth Sci Front* 17:140–145 (in Chinese with English abstract)
- Wang XX, Wang T, Qi QJ, Li S (2011) Temporal-spatial variations, origin and their tectonic significance of the Late Mesozoic granites in the Qinling, Central China. *Acta Petrol Sin* 27:1573–1593 (in Chinese with English abstract)
- Wei JH, Liu CQ, Zhao YX, Li ZD (2001) Time span of the major ore-forming stages of the Wulong gold deposit, Liaoning. *Geol Rev* 47:433–437 (in Chinese with English abstract)
- Wiedenbeck M, Alle P, Corfu F, Griffin WL, Meier M, Oberli F, Quadt A, Roddick JC, Spiegel W (1995) Three natural zircon standards for U-Th-Pb, Lu-Hf, trace element and REE analyses. *Geostand Geoanalytical Res* 19:1–23
- Wu FY, Lin JQ, Wilde SA, Zhang XO, Yang JH (2005) Nature and significance of the Early Cretaceous giant igneous event in eastern China. *Earth Planet Sci Lett* 233:103–119
- Xu QD, Zhong ZQ, Zhou HW, Yang FC, Tang XC (1998) $^{40}\text{Ar}/^{39}\text{Ar}$ dating of the Xiaqingling gold area in Henan Province. *Geol Rev* 44:323–327 (in Chinese with English abstract)
- Xu YG, Huang XL, Ma JL, Wang YB, Iizuka Y, Xu JF, Wang Q, Wu XY (2004) Crust-mantle interaction during the tectono-thermal reactivation of the North China Craton: constraints from SHRIMP zircon U-Pb chronology and geochemistry of Mesozoic plutons from western Shandong. *Contrib Mineral Petrol* 147:750–767
- Xu XS, Griffin WL, Ma X, O'Reilly SY, He ZY, Zhang CL (2009) The Taihua group on the southern margin of the North China craton: further insights from U-Pb ages and Hf isotope compositions of zircons. *Mineral Petrol* 97:43–59
- Xue LW, Yuan ZL, Zhang YS, Qiang LZ (1995) The Sm-Nd isotope age of Taihua Group in Lushan area and their implications. *Geochemica* 24:92–97 (in Chinese with English abstract)
- Yan JS, Pang ZS, Yue ZS, Zhang ZH (2005) The tectonic characteristics of Machaoying fault zone and studies of gold mineralization. Yellow River Conservancy Press, Zhengzhou, in Chinese
- Yan DP, Zhou MF, Zhao DG, Li JW, Wang GH, Wang CL, Qi L (2010) Origin, ascent and oblique emplacement of magmas in a thickened crust: an example from the Cretaceous Fangshan adakitic pluton, Beijing. *Lithos* 123:102–120
- Yang JH, Zhou XH, Chen LH (2000) Dating of gold mineralization for super-large altered tectonite-type gold deposits in Northwestern Jiaodong Peninsula and its implications for gold metallogeny. *Acta Petrol Sin* 16:454–458 (in Chinese with English abstract)
- Yang JH, Wu FY, Wilde SA (2003) A review of the geodynamic setting of large-scale Late Mesozoic gold mineralization in the North China Craton: an association with lithospheric thinning. *Ore Geol Rev* 23:125–152
- Yang JH, Wu FY, Chung SL, Lo CH, Wilde SA, Davis GA (2007) Rapid exhumation and cooling of the Liaonan metamorphic core

- complex: Inferences from $^{40}\text{Ar}/^{39}\text{Ar}$ thermochronology and implications for Late Mesozoic extension in the eastern North China Craton. *Geol Soc Am Bull* 119:1405–1414
- Yao JM, Zhao TP, Li J, Sun YL, Yuan ZL, Chen W, Han J (2009) Molybdenite Re-Os age and zircon U-Pb age and Hf isotope geochemistry of the Qiyugou gold system, Henan Province. *Acta Petrol Sin* 25:374–384 (in Chinese with English abstract)
- Ye HS, Mao JW, Xu LG, Gao JJ, Xie GQ, Li XQ, He CF (2008) SHRIMP zircon U-Pb dating and geochemistry of the Taishanmiao aluminous A-type granite in Western Henan Province. *Geol Rev* 54:699–711 (in Chinese with English abstract)
- Yu JJ, Mao JW (2004) $^{40}\text{Ar}/^{39}\text{Ar}$ Dating of albite and phlogopite from porphyry iron deposits in the Ningwu basin in east-central China and its significance. *Acta Geol Sin(Engl Ed)* 78:435–442
- Zhang YG, Frantz JD (1987) Determination of the homogenization temperatures and densities of supercritical fluids in the system NaCl-KCl-CaCl₂-H₂O using synthetic fluid inclusions. *Chem Geol* 64:335–350
- Zhang JJ, Zheng YD (1999) The multiphase extension and their ages of the Xiaolinling metamorphic core complex. *Acta Geol Sin* 73:139–147
- Zhang XO, Cawood PA, Wilde SA, Liu RQ, Song HL, Li W, Snee LW (2003) Geology and timing of mineralization at the Cangshang gold deposit, north-western Jiaodong Peninsula, China. *Miner Deposita* 38:141–153
- Zhang HF, Sun M, Zhou XH, Ying JF (2005) Geochemical constraints on the origin of Mesozoic alkaline intrusive complexes from the North China Craton and tectonic implications. *Lithos* 81:297–317
- Zhang YH, Zhang SH, Han YG, Zhang HJ (2006) Strik-slip features of the Machaoying fault zone and its evolution in the Huaxiong terrane, Southern North China Craton. *J Jilin Univ (Earth Sci Ed)* 36:169–193 (in Chinese with English abstract)
- Zhang J, Zhang HF, Kita N, Shimoda G, Morishita Y, Ying JF, Tang YJ (2011) Secular evolution of the lithospheric mantle beneath the eastern North China craton: evidence from peridotitic xenoliths from Late Cretaceous mafic rocks in the Jiaodong region, east-central China. *Int Geol Rev* 53:182–211
- Zhao GC, Sun M, Wilde SA, Li SZ (2004) A Paleo-Mesoproterozoic supercontinent: assembly, growth and breakup. *Earth Sci Rev* 67:91–123
- Zhao GC, He YH, Sun M (2009) The Xiong'er volcanic belt at the southern margin of the North China Craton: petrographic and geochemical evidence for its outboard position in the Paleo-Mesoproterozoic Columbia Supercontinent. *Gondwana Res* 16:170–181
- Zheng JM, Xie GQ, Liu J, Chen MH, Wang SM, Guo SF, Gao X, Li GD (2007) $^{40}\text{Ar}/^{39}\text{Ar}$ dating of phlogopite from the Xishimen skarn iron deposit in the Handan-Xingtai area, Southern Hebei, and its implications. *Acta Petrol Sin* 23:2513–2518 (in Chinese with English abstract)
- Zhou HS, Ma CQ, Zhang C, Chen L, Zhang JY, Yu ZB (2008) Yanshanian aluminous A-type granitoids in the Chunshui of Biyang, south margin of North China Craton: implications from petrology, geochronology and geochemistry. *Acta Petrol Sin* 24:49–64 (in Chinese with English abstract)
- Zhou K, Ye HS, Mao JW, Qu WJ, Zhou SF, Meng F, Gao YL (2009) Geological characteristics and molybdenite Re-Os isotope dating of Yuchiling porphyry Mo deposit in Western Henan Province. *Mineral Deposits* 28:170–184 (in Chinese with English abstract)
- Zhu G, Xie CL, Xiang BW, Hu ZQ, Wang YS, Li X (2007) Genesis of the Hongzhen metamorphic core complex and its tectonic implications. *Sci China Ser D Earth Sci* 50:649–659
- Zhu G, Xie CL, Chen W, Xiang BW, Hu ZQ (2010) Evolution of the Hongzhen metamorphic core complex: evidence for Early Cretaceous extension in the eastern Yangtze craton, eastern China. *Geol Soc Am Bull* 122:506–516